Food Bioscience 62 (2024) 105088

Contents lists available at ScienceDirect

Food Bioscience

journal homepage: www.elsevier.com/locate/fbio

A multifunctional natural treasure based on a "one stone, many birds" strategy for designing health-promoting applications: *Tordylium apulum*

Nilofar [a,b], Gokhan Zengin [a,*], Abdullahi Ibrahim Uba [c], Nurgul Abul [d], Ilhami Gulcin [d], Ismail Koyuncu [e], Ozgur Yuksekdag [e], Sathish Kumar M Ponnaiya [f], Surendar Tessappan [f], Filomena Nazzaro [g], Florinda Fratianni [g], Francesca Coppola [g], Alina Kalyniukova [h], Gizem Emre [i], Vasil Andruch [j]

[a] *Physiology and Biochemistry Laboratory, Department of Biology, Science Faculty, Selcuk University, Konya, 42130, Turkey*
[b] *Department of Pharmacy, Botanic Garden "Giardino dei Semplici", Università degli Studi "Gabriele, Chieti, Italy*
[c] *Department of Molecular Biology and Genetics, Istanbul AREL University, Istanbul, 34537, Turkey*
[d] *Department of Chemistry, Science Faculty, Ataturk University, Erzurum, Turkey*
[e] *Department of Medical Biochemistry, Faculty of Medicine, Harran University, Sanliurfa, 63290, Turkey*
[f] *Ponnaiya's Code and Genome Pvt Ltd, Madurai, 625012, India*
[g] *Institute of Food Science, Italian National Research Council, Via Roma 64, 83100, Avellino, Italy*
[h] *Faculty of Forestry and Wood Sciences, Czech University of Life Sciences Prague, Kamýcká 129, CZ - 165 21, Praha 6 - Suchdol, Czech Republic*
[i] *Department of Pharmaceutical Botany, Faculty of Pharmacy, Marmara University, Istanbul, Turkey*
[j] *Department of Analytical Chemistry, Institute of Chemistry, Faculty of Science, P. J. Šafárik University, 041 80, Košice, Slovakia*

ARTICLE INFO

Keywords:
Tordylium apulum
Diabetes mellitus
Carbonic anhydrase
Apoptosis
Anti-biofilm
Versatile agents

ABSTRACT

Wild plants provide important bioactive compounds, and their analysis relies heavily on selecting the right extraction techniques and solvents. This study was conducted to determine the phenolic content and biopharmaceutical potential of four different extracts (ethyl acetate, ethanol, 70% ethanol, and water) from the aerial parts of wild plant *Tordylium apulum* L. The biochemical profile of the extract was screened using high performance liquid chromatography -mass spectrometry (HPLC-MS) analysis. The total phenolic and flavonoid content was examined using the Folin-Ciocalteu assay and the aluminium trichloride assay, respectively. The antioxidant activity was evaluated through several tests, including 2,2-Diphenyl-1-picrylhydrazyl (DPPH), 2,2′-azino-bis(3-ethylbenzothiazoline-6-sulfonic acid) (ABTS), cupric reducing antioxidant capacity (CUPRAC), ferric reducing antioxidant power (FRAP), phosphomolybdenum (PBD), and metal chelating activity (MCA). Five types of enzyme inhibition activity were tested against acetylcholinesterase (AChE), butrylcholinesterase (BChE), tyrosinase, α-amylase, and α-glucosidase. Additionally, For the first time, the inhibitory activity of *T. apulum* extract against human carbonic anhydrase isoenzymes I and II (hCA-I and hCA-II) was evaluated. Fifty-five compounds for negative ionization mode, and twenty-eight compounds for positive ionization mode were recorded in HPLC-MS analysis and they were polyphenolic, flavonoids, carbohydrates, sugar alcohol and amino acids. These results indicate that different solvents extract varying levels of antioxidants from *T. apulum*, with ethanol and water extracts generally exhibiting superior antioxidant activities. The ethanol extract of *T. apulum* exhibited the maximum contents of total phenolics measuring 33.71 mg gallic acid equivalent (GAE)/g. The ethanol extract exhibited the highest inhibition of AChE with 2.28 mg galanthamine equivalent (GALAE)/g. The ethyl acetate and ethanol extracts also showed the highest hCA-I and hCA-II inhibition potential, respectively. The ethanol-water and water extracts acted on the biofilm of *E. coli* (49.93% and 45.22%, respectively), and the biofilm of *P. aeruginosa* (50.68% and 44.46%, respectively). The extracts were tested on different cell lines for cytotoxic potentials and in particular the water extract induced the apoptotic pathways in cervical cancer (HELA) cell lines. In conclusion, *T. apulum* exhibit multidirectional biological properties and it could be considered as a versatile agent for the development of health-promoting applications.

* Corresponding author.
E-mail address: biyologzengin@gmail.com (G. Zengin).

https://doi.org/10.1016/j.fbio.2024.105088
Received 18 August 2024; Received in revised form 7 September 2024; Accepted 9 September 2024
Available online 10 September 2024

1. Introduction

Plants are valuable source of bioactive compounds (Bernhoft, 2010; Sinan et al., 2024; Smith, 2003). The analysis of these compounds from plant materials largely depends on the choice of appropriate extraction methods (Azwanida, 2015; Nilofar et al., 2024; Sasidharan et al., 2011; Smith, 2003) and extraction solvents (Anwar & Przybylski, 2012). Researchers have used solvents like methanol, ethanol, hexane, ethyl alcohol and many other polar and non-polar solvent to efficiently extract bioactive compounds from plant parts, highlighting the importance of solvent polarity in isolating these compounds. (Anwar & Przybylski, 2012; Sasidharan et al., 2011; Smith, 2003; Wong & Kitts, 2006). Ngo et al. found that 50% ethanol and 50% acetone was optimal for extracting solids, phenolics, and flavonoids from *Salacia chinensis* using ultrasonic methods (Ngo et al., 2017). While, Koffi et al. discovered that ethanol extracted higher amounts of phenolic contents from walnut fruits more effectively than methanol, acetone, or water (Koffi et al., 2010). On the other hand, Ahmed et al. discovered that the 50% methanol and methanol extracts contained the highest levels of phenolic compounds and exhibited the most effective scavenging and reducing abilities (Ahmed et al., 2023). Altemimi et al. claimed that the polarity of common solvents ranges from least to most polar: Hexane < Chloroform < Ethyl acetate < Acetone < Methanol < Water (Altemimi et al., 2017). These natural products are known to exhibit various biological activities. In recent years, there has been growing interest in testing the antioxidant properties of natural products, primarily because an antioxidant-rich diet is believed to offer significant health benefits. These antioxidants scavenge reactive oxygen species (ROS) and affect processes related to free radical-induced damage (Whang et al., 2005). Antioxidants help lower the risk of chronic diseases, including cardiovascular, neurological diseases, diabetes, cancer, hypertension, and skin and blood-related conditions (Bjørklund & Chirumbolo, 2017; Jideani et al., 2021; Ponnanikajamideen et al., 2019).

In the Mediterranean region, ethnobotanical studies have discovered around 2300 wild plant and fungi species that are still harvested and eaten as food (Hadjichambis et al., 2008). Despite a decline, these wild edible plants remain commonly consumed in many areas due to their health benefits, taste, and cultural significance (Dogan et al., 2004; Ghirardini et al., 2007; Guarrera & Savo, 2016; Luczaj et al., 2012). *Tordylium apulum* L., a species within the Apiaceae family (Apioideae), is found in nearly all countries bordering the Mediterranean (Maresca et al., 2024; Tirillini et al., 2006). This plant genus has been extensively researched in Italy, Greece, and Turkey, particularly focusing on its essential oil composition, as highlighted in several studies (Tirillini et al., 2006; Tosun et al., 2006; Özek et al., 2007). Moreover, coumarins (bergaptene, cnidiadin, umbelliferone, *R*-meranzin, isoimperatorin, 7-prenylum-belliferone and 2′(*S*),3′(*R*)-2′-acetoxyisopropyl-3′-acetoxy-2′, 3′-dihydroangelicin). Extracted from this plant has shown promising anticancer properties. Notably, it has been found to exhibit anticancer activity against non-small cell bronchial carcinoma, suggesting its potential as a therapeutic agent in the treatment of this type of lung cancer (Kofinas, Chinou, Loukis, Harvala, Roussakis, et al., 1998). In a recent study by Maresca et al. (2024), the essential oil of *T. apulum* was examined for chemical composition and biological activities and found the *β-cis*-ocimene (65.0%) and octyl hexanoate (14.4%) were predominant compounds. *Tordylium* genus also exhibits notable in vitro antioxidant and antimicrobial activities, as documented in some previous studies, suggest effectiveness against a range of pathogenic bacteria (Kofinas et al., 1993; MatejiÄ et al., 2013). This discovery adds significant value to the plant's medicinal uses and underscores the importance of continued research into its bioactive components.

Consequently, the study aimed to (i) examine bioactive compounds from the aerial parts of *T. apulum* using different extraction solvents, (ii) evaluate and compare the total phenolic content, flavonoid content and antioxidant capacity, (iii) Investigate the enzyme inhibitory properties of the extracts, (iv) explore the effectiveness of antimicrobials/antibiofilms, (v) identify cytotoxic properties in different cell lines, and (vi) understand the interaction between the phytochemical compounds and the biological activities of the extracts molecular docking and network pharmacological approaches.

2. Materials and methods

2.1. Plant collection

In 2021, plant materials were gathered from Maltepe location (Başıbüyük), Istanbul, Turkey. Dr. Gizem Emre performed the taxonomic identification, and a voucher specimen was stored in the herbarium of Marmara University (Voucher number: MARE-22679). The aerial portions were separated, dried in the shade at room temperature, powdered, and then stored away from light.

2.2. Plant extract preparation

The extraction process involved four solvents: ethyl acetate, ethanol, ethanol/water (70%), and water. Each sample, weighing 10 g, was macerated with 200 mL of ethyl acetate, ethanol, and ethanol/water for a 24-h period at room temperature. The water extract was created by steeping 10 g of plant material in boiled water for 15 min. Organic solvents were evaporated under reduced pressure, and the water extract underwent freeze-drying.

2.3. Assay for total phenolic and flavonoid contents

Following the procedures specified by (Slinkard & Singleton, 1977), total phenolics and flavonoids were measured. Gallic acid (GA) and rutin (RE) were employed as references in the experiments, with the results presented as gallic acid equivalents (GAE) and rutin equivalents.

2.4. LC-MS-qTOF metabolomic analysis

Metabolomic analysis was performed using an Agilent 1290 Infinity II system coupled with an Agilent 6546 L C/MS QTOF instrument (Agilent, USA). Separation was achieved using an InfinityLab Poroshell 120 EC-C18 column (2 × 150 mm, 2.7 μm) from Agilent (USA). The analytical details are given in the supplemental materials (Duran et al., 2024).

2.5. Assays for in vitro antioxidant capacity

As per the procedures outlined in our previous paper (Grochowski et al., 2017), various antioxidant assays were executed. The outcomes from the DPPH, ABTS radical scavenging, CUPRAC, and FRAP assays were reported in milligrams of Trolox equivalents (TE) per gram of extract. The phosphomolybdenum (PBD) assay indicated the antioxidant potential in millimoles of Trolox equivalents (TE) per gram of extract, while the metal chelating activity (MCA) was expressed in milligrams of disodium edetate equivalents (EDTAE) per gram of extract.

2.6. Inhibitory effects against some key enzymes

In accordance with the established protocols (Grochowski et al., 2017), enzyme inhibition experiments were conducted on the samples. The activities inhibiting amylase and glucosidase were expressed in acarbose equivalents (ACAE) per gram of extract, whereas inhibition of acetylcholinesterase (AChE) and butyrylcholinesterase (BChE) was measured in milligrams of galanthamine equivalents (GALAE) per gram of extract. Tyrosinase inhibition was calculated in milligrams of kojic acid equivalents (KAE) per gram of extract.

The carbonic anhydrase (hCA I-II) isoenzymes used in the experiments were purified from human erythrocyte cells using Sepharose-4B-L-Tyrosine sulfanilamide affinity chromatography according to the

previously reported method (Kucukoglu et al., 2019; Özbey et al., 2016). The esterase method was used for enzyme activity determination. According to this method, the change in absorbance caused by the hydrolysis of the substrate (p-nitrophenylacetate, PNFA) to p-nitrophenolate and acetate by hCA I-II isoenzymes at 25 °C for 3 min was determined spectrophotometrically at 348 nm (Tugrak et al., 2021). The change in activity by adding different inhibitor concentrations to the enzyme activity measurement mixture consisting of 0.05 M Tris-SO_4 buffer (pH 7.4), 3 mM PNFA and water was shown with % Activity-Concentration graph (IC_{50}). The inhibitor concentration that reduced enzyme activity by 50% was determined from the obtained graph. Acetazolamide (AAZ), clinically used in hCA inhibition, was also studied as a standard inhibitor.

2.7. Antimicrobial evaluation

2.7.1. Minimal inhibitory concentration

For MIC determination, the resazurin microtiter plate assay was applied using flat-bottomed 96-well microplates, followed by incubation at 37 °C for 24 h (with A. baumannii grown at 35 °C under identical conditions) (Fratianni et al., 2023). Sterile DMSO and tetracycline (dissolved in DMSO, 7 μg/mL) served as negative and positive controls, respectively. All tests were conducted in triplicate, with results presented as the mean ± standard deviation.

2.8. The antibiofilm activity

2.8.1. Crystal violet test

The capacity of the extracts and water-infuse of *T. apulum* to affect the bacterial biofilm formation was evaluated using flat-bottomed 96-well microtiter plates (Falcon, VWR International, Milano, Italy) (Fratianni et al., 2023). Ten microliters of the overnight bacterial cultures (adjusted to 0.5 McFarland with fresh culture broth), were brought in each well with10 μg/mL or 20 μg/mL of samples and sterile Luria–Bertani broth (LB, Sigma Aldrich Italia, Milano, Italy) to a final volume of 250 μL. The plates were covered with parafilm tape and incubated for 48 h. Following the eliminating of the planktonic cells, sessile cells were slightly twice-washed with sterile phosphate buffered saline (PBS). After 10 min 200 μL of methanol was included to each well for 15 min to let the fixation of the sessile cells. The dryness of plates was followed by the addition of 200 μL of 2% w/v crystal violet solution to each well. The staining solution was eliminated after 20 min, then the plates were slightly cleaned with sterile PBS and left to dry. 200 μL of glacial acetic acid 20% w/v were added to allow the release of the bound dye. The absorbance was measured at λ = 540 nm (Cary 50 Bio, Varian). The adhesion percentage was determined in comparison to the control (bacterial cells cultured without samples, with a 0% inhibition rate). Each experiment was performed three times, and the findings were expressed as the mean ± SD.

2.8.2. MTT test

The effect of two concentrations, 10 and 20 μg/mL of the extracts and water-infuse of *T. apulum* was also assessed by evaluating their action on the metabolic activity of the bacterial cells. The measurement was performed through the 3-(4,5-dimethylthiazol-2-yl)-2,5-diphenyltetrazolium bromide (MTT) colorimetric method (Fratianni et al., 2023). After 48 h total of incubation, we removed the planktonic cells, and in each well we added 150 μL of PBS and 30 μl of 0.3% of MTT (Sigma, Milano, Italy). The MTT solution was eliminated after 2 h of incubation, and two washing steps were made with 200 μL of sterile PBS. The addition of 200 μL of DMSO let the dissolution of the formazan crystals that were measured at λ = 570 nm (Cary 50 Bio Varian) after 2 h.

2.9. Cytotoxicity

2.9.1. Cell culture

For this study, the following cell lines were sourced from ATCC and preserved in liquid nitrogen: DU-145 (Prostate Carcinoma), MDA-MB-231 (Breast Adenocarcinoma), HELA (Cervix Adenocarcinoma), A549 (Lung Carcinoma), and HUVEC (Endothelial Cells). Cells were maintained in DMEM-F12/RPMI-1640 media, enriched with 10% Fetal Bovine Serum (FBS), 100 μg/mL streptomycin, and 100 IU/mL penicillin, within incubators set to 37 °C, 5% CO2, and humid conditions.

2.9.2. Cell viability assay

To evaluate the cytotoxicity of *T. apulum* extracts, the MTT assay (3-(4,5-Dimethylthiazol-2-yl)-2,5-Diphenyltetrazolium Bromide) was conducted. Cells (DU-145, MDA-MB-231, HELA, A549, and HUVEC) were seeded at 1×10^4 cells per well in a sterile 96-well plate and incubated for 24 h. After media removal, the cells were treated with extracts (0–200 μg/mL) for another 24 h. MTT reagent (10 μL, 0.5 mg/mL) was then added, followed by a 4-h incubation. The media was replaced with 100 μL of DMSO, and absorbance was measured at 570 and 690 nm using a plate reader. The IC_{50} values were calculated based on these measurements.

2.9.3. Apoptotic effect of the water extract on HELA cancer cell with acridine orange/ethidium bromide (AO/EB) staining

It was used to morphologically detect the apoptosis of the water extract (30 μg/mL) applied to HELA cells. The extract-treated cell was washed with PBS after incubation and fixed with 70% ethanol. At the end of fixation, the cells were washed with distilled water, stained with Acridine orange/Ethidium bromide (Cat No./ID: A6014-E1510) (Sigma Aldrich, Germany) working solution, and images were taken under a fluorescence microscope.

2.9.4. Apoptotic effect of the water extract on HELA cancer cell with annexin V

To evaluate the apoptotic effects of the water extract, the FITC Annexin V Apoptosis Detection Kit I (BD Biosciences, New Jersey, USA) was utilized according to the manufacturer's instructions. Cell HELA was plated in 6-well plates (5×10^5 cells/well) and after 24 h of incubation, a concentration of substance 4 of 30 μg/mL was applied, followed by 24 h of incubation. Cells were grown using trypsin and transferred to new 1106-inch tubes in 1X binding buffer. The tubes were incubated at room temperature for 15 min, after which 5 μL of fluorochrome-conjugated Annexin V and 5 μL of Propidium Iodide were added. Subsequently, 100 μL of 1X binding buffer was introduced, and the cells were centrifuged at 851×*g* at 4 °C for 5 min. Finally, the cells were analyzed by flow cytometry (BD, New Jersey, USA).

2.9.5. Molecular modeling

The following 3D structures of proteins were retrieved from the Protein Data Bank (PDB) (https://www.rcsb.org/) (Kurumbail et al., 1996): crystal complexes of human AChE with donepezil (PDB ID: 7E3H) (Dileep et al., 2022), human BChE with AI0 (PDB ID: 7Q3Q) (Knez et al., 2023), human α-amylase with acarbose (PDB ID: 1B2Y) (Nahoum et al., 2000), Bcl-2 with Navitoclax analog (PDB ID: 4MAN) (Souers et al., 2013), CDK2/Cyclin A with AZD5438 (PDB ID: 6GUE) (Wood et al., 2019), and TRAF2 with Wee1Chk1 inhibitor (PDB ID: 2 × 7F). Also, the homology model of human tyrosinase and glucosidase enzymes built in our previous study (Omer et al., 2022) was retrieved. These proteins were prepared using the PrepareProtein toolkit on the Playmolecule server (https://www.playmolecule.com/), where the pKa of the titratable residues in each protein was computed and used to protonate the protein (Martínez-Rosell et al., 2017). Similarly, all ligand 3D structures were retrieved from the PubChem database (https://pubchem.ncbi.nlm.nih.gov/) (Pettersen et al., 2004) and minimized using UCSF Chimera (Pettersen et al., 2004). To generate a docking grid

Table 1
Extraction yields (%) and total phenolic (TPC) and flavonoid (TFC) contents in the tested extracts[a].

Extracts	Extraction yields (%)	TPC (mg GAE/g)	TFC (mg RE/g)
Ethyl acetate	2.98	26.84 ± 1.29[c]	4.18 ± 0.17[d]
Ethanol	10.54	33.71 ± 0.14[a]	28.49 ± 0.43[c]
Ethanol/Water (70%)	14.76	29.15 ± 0.73[b]	37.90 ± 0.07[a]
Water (infused)	14.31	32.52 ± 0.65[a]	32.32 ± 0.20[b]

[a] Values are reported as mean ± SD of three parallel measurements. GAE: Gallic acid equivalents; RE: Rutin equivalents. Different letters indicate significant differences between the tested extracts ($p < 0.05$).

using AutoDockTools (ADT), each the cocrystal ligand served as a reference ligand with the following coordinates: AChE (X: 5.01, Y: 35.37, Z: −8.38 Å), BChE (X: 42.16, Y: −17.91, Z: 42.72 Å), α-amylase (X: −1.54, Y: −44.04, Z: 22.63 Å), tyrosinase (X: 29.99, Y: 18.21, Z: 96.45 Å), glucosidase (X: −13.77, Y: 24.04, Z: 12.35 Å), BCL-2 (X: 16.58, Y: 5.28, Z: 0.62 Å), CDK2 (X: −6.92, Y: −26.08, Z: 9.78 Å), and TRAF2 (X: 22.03, Y: 0.24, Z: 52.68 Å) all placed in a grid box of dimensions X: 45, Y: 45, Z: 45 Å. Gasteiger partial charges were added to all atoms after merging all hydrogen atoms. Docking was carried out using AutoDock 4.2.6 (https://autodock.scripts.edu) (Morris et al., 2009), employing the Lamarckian genetic algorithm for ligand conformational search with the number of runs set to 10. Finally, the protein-ligand interaction was examined using a Maestro Viewer (Schrodinger Inc.).

2.9.6. Network pharmacology

We obtained LC-MS data and identified 63 components in the extract of *T. apulum*. The plant has been reported as antioxidant (Maresca et al., 2024), so coronary artery and Alzheimer's were taken for the network pharmacology analysis, the analysis was done using canonical SMILES and the structures were retrieved from PubChem (Kim et al., 2023). SwissTargetPrediction tool was used to predict the compound targets, which calculates user's query compounds and those compiled in curated, cleansed of known actives (Daina et al., 2019). The Compound targets were selected based on the probability score ≥0.1 and the standardization of target genes and gene symbols UniProt was used. Then, Open target platform (https://platform.opentargets.org/) was used to retrieve data to find the potential targets for Coronary artery (ID: EFO_0001645) and Alzheimer's disease (ID: MONDO_0004975), the target compounds with overall probability score ≥0.5 were taken for the analysis. The common targets were identified and collected by construction Venn diagram using Venny 2.1.0, Venn diagram was constructed for both the disease. Cytoscape version 3.10.2 was used for the construction and visualization of compound's target (Shannon et al., 2003). The tool used for construction of Protein-Protein interaction (PPI) network is Search Tool for Recurring Instances of Neighbouring Genes/Proteins (STRING) database (Szklarczyk et al., 2019). The PPI network for constructed for both the disease each contained a set of 29 and 13 compound genes respectively, with a stringent interaction threshold set to "high confidence >0.7". For further analysis, we imported this network to Cytoscope where the network was constructed using confidence-based approach. The hub genes were identified using Cytohubba plugin. ShinyGO 0.80 is a web-based tool for analysing gene sets and performing functional enrichment analysis. It allows users to input a set of genes KEGG pathways, biological process, cellular components and molecular function. Here, the common targets of disease and *T. apulum* compound's target were uploaded in the ShinyGO 0.80 for the prediction of Gene Ontology and KEGG pathway (Ge et al., 2020). As stated by Luo & Brouwer in 2013 and Kanehisa et al., in 2020 tool allows users to input a set of genes and the top 10 KEGG pathways, biological process, cellular components and molecular function were identified and selected for plotting graph, which provides insight into fold enrichment, Genome plot is retrieved which as well contains genomic location information. Swiss SDME is a web tool used to make predictive models of physicochemical properties, pharmacokinetics, drug likeness, etc. We retrieved physicochemical and pharmacokinetic properties of the compound using Swiss ADME, with canonical SMILES as the input (Daina et al., 2019). This comprehensive analysis has delved into various physical and chemical properties of the compound i.e., number of heavy atoms, number of rotatable bonds, topological polar surface area, molecular refractivity, and etc. Additionally, we have examined the pharmacokinetic properties of compound e.g. P-glycoprotein substrate, gastro-intestinal absorption and others.

2.9.7. Statistical analysis

The results were given as mean ± SD of three parallel experiments. Differences in extract levels among the extracts were assessed using ANOVA with Dunnet's test ($p < 0.05$). GraphPad 9.0 was used for all analyses.

3. Results and discussion

3.1. Total phenolic and total flavonoid contents

Tordylium apulum is rich in phenolic and flavonoid compounds (Kofinas, Chinou, Loukis, Harvala, Maillard, et al., 1998; Maresca et al., 2024). The analysis of the total phenolic content (TPC) and total flavonoid content (TFC) of the aerial parts of the *T. apulum* across various extraction solvents reveals notable differences (Table 1). For TPC, the ethanol extract exhibited the highest value at 33.71 mg GAE/g followed by 70% ethanol 29.15 mg GAE/g, while the ethyl acetate extract showed the lowest value at 26.84 mg GAE/g. Regarding TFC 70% ethanol extract contained the highest content at 37.90 mg RE/g, significantly higher than the ethyl acetate extract, which has the lowest TFC at 4.18 mg RE/g (Table 1). The water extract exhibited the second highest TFC 32.32 mg RE/g. A previous study found that polar extracts of *T. aegyptiacum* L. recorded flavonoid content, measuring 244.3 mg CE/g, which represented the highest among the other tested plants (Christou et al., 2024). These results align with earlier studies showing that 70% ethanol extracts contain higher levels of flavonoids (Banjarnahor & Artanti, 2014; Lazarova et al., 2024; Zengin et al., 2023). This discovery reinforces the current research and further validates the use of 70% ethanol as an effective solvent for flavonoid extraction. This suggests that these solvents are particularly effective in extracting flavonoids, which are known for their beneficial antioxidant properties (Banjarnahor & Artanti, 2014). These results indicate that the choice of solvent greatly influences the extraction efficiency of phenolic and flavonoid compounds from the aerial parts of the *T. apulum*.

3.2. Metabolomic analysis

A total of 350 entities were identified in the metabolomic analysis of the four *T. apulum* extracts. By applying a frequency filter with a 75% threshold, the final dataset was narrowed down to 55 entities in negative ionization mode and 28 in positive ionization mode (Table 2). This refinement facilitated the creation of a principal component analysis (PCA) model, which demonstrated distinct clustering of samples depending on the extraction solvent used (Fig. S1 for negative ionization mode and Fig. S2 for positive ionization mode). For multivariate group analysis, partial least squares-discriminant analysis (PLS-DA) was employed to distinguish plant extracts. Using the variable importance in projection (VIP) score and analysis of variance (ANOVA, $p < 0.05$), the most significant features responsible for metabolite differentiation in extracts were identified. Figs. S1 and S2 presents the top 15 metabolites validated by the VIP score. Group classification via PCA and PLS-DA was further corroborated by a heatmap, which illustrated the distinctions between the metabolite profiles in the four plant extracts (Fig. S2) for negative ionization mode and Fig. S3 for positive ionization mode). The identified compounds belong to polyphenolic, flavonoids,

Table 2
The identified compounds in negative and positive ion mode.

N°	Compound	ESI	Formula	Mass	m/z	Retention Time
Negative ionization mode						
1	N-hexosyl-L-asparagine	[M-H]⁻	$C_{10}H_{18}N_2O_8$	294.1065	293.0093	1.278
2	Liqcoumarin	[M-H]⁻	$C_{12}H_{10}O_4$	218.056	217.0487	1.296
3	D-Mannitol	[M-H]⁻	$C_6H_{14}O6$	182.0792	181.0719	1.301
4	Gluconic/Galactonic acid	[M-H]⁻	$C_6H_{12}O_7$	196.0583	195.0511	1.305
5	N-(1-Deoxy-1- hexosyl)threonine	[M-H]⁻	$C_{10}H_{19}NO_8$	281.1111	280.1039	1.312
6	L-Xylonate	[M-H]⁻	$C_5H_{10}O_6$	166.0478	165.0101	1.313
7	Saccharide	[M-H]⁻	$C_{12}H_{22}O_{11}$	342.1162	341.0879	1.347
8	N-(1-Deoxy-1 hexosyl)proline	[M-H]⁻	$C_{11}H_{19}NO_7$	277.1163	276.1089	1.377
9	Coriose	[M-H]⁻	$C_7H_{14}O_7$	210.0742	209.0668	1.387
10	L-Arabinose	[M-H]⁻	$C_6H_{10}O_5$	150.0529	149.0457	1.431
11	L-Malic acid	[M-H]⁻	$C_4H_6O_5$	134.0216	133.0143	1.535
12	N-(1-Deoxy-1- hexosyl)valine	[M-H]⁻	$C_{11}H_{21}NO_7$	279.1318	278.1246	1.643
13	L-Valine	[M-H]⁻	$C_5H_{11}NO_2$	117.079	116.0718	1.646
14	D-Pipecolic acid	[M-H]⁻	$C_6H_{11}NO_2$	189.1002	188.0930	1.647
15	Pyroglutamic acid	[M-H]⁻	$C_5H_7NO_3$	129.0427	128.0354	1.914
16	N-(1-Deoxy-1- hexosyl)isoleucine	[M-H]⁻	$C_{12}H_{23}NO_7$	293.1475	292.1404	2.516
17	Salicylic acid-*β*-D-glucoside	[M-H]⁻	$C_{13}H_{16}O_8$	300.0846	299.0775	3.462
18	D-Phenylalanine	[M-H]⁻	$C_9H_{11}NO_2$	165.0791	164.0781	4.173
19	Pantothenic acid	[M-H]⁻	$C_9H_{17}O_5N$	219.1108	218.1035	4.81
20	*p*-Coumaric acid glycoside derivate 1	[M-H]⁻	$C_{20}H_{26}O_{12}$	458.1424	457.1354	8.125
21	Hydroxyquinaldic acid	[M-H]⁻	$C_{10}H_7NO_3$	189.0427	188.0201	8.465
22	*p*-Coumaroyl-D-hexose	[M-H]⁻	$C_{15}H_{18}O_8$	326.1004	325.0931	8.876
23	Trihydroxybenzene	[M-H]⁻	$C_6H_6O_3$	252.0635	251.0562	9.661
24	*p*-Coumaric acid glycoside derivate 2	[M-H]⁻	$C_{20}H_{26}O_{12}$	458.1425	457.1353	9.792
25	Trimethoxycoumarin	[M-H]⁻	$C_{12}H_{12}O_5$	282.0741	281.0668	9.938
26	*O*-Feruloyl-*β*-D-hexose	[M-H]⁻	$C_{16}H_{20}O_9$	356.1108	355.01001	10.016
27	Kaempferol-*O*-*β*-D-hexosyl-(1 2)-β–hexosyl-(1–2)-*β*-D-hexoside	[M-H]⁻	$C_{33}H_{40}O_{21}$	772.2062	771.1994	10.033
28	*p*-Coumaroyl quinic acid	[M-H]⁻	$C_{16}H_{18}O_8$	338.1003	337.0931	10.41
29	*O*-Feruloylquinic acid	[M-H]⁻	$C_{17}H_{20}O_9$	368.1108	367.1035	11.037
30	Isorhamnetin-(hexose-deoxyhexose)-hexose	[M-H]⁻	$C_{33}H_{40}O_{20}$	756.2114	755.1203	11.259
31	Isorhamnetin-*O*-[*β*-D-hexosyl-(1–2)-*α*-L-deoxyhexosyl-*β*-D-hexoside]	[M-H]⁻	$C_{34}H_{42}O_{21}$	786.2215	785.2145	11.625
32	Hydroxycoumarin	[M-H]⁻	$C_9H_6O_3$	162.0318	161.0245	11.678
33	Plumieride	[M-H]⁻	$C_{21}H_{26}O_{12}$	470.1424	469.1353	12.523
34	Quercetin -[deoxyhexosyl-(1–2)-deoxyhexosyl-(1–6)-hexoside]	[M-H]⁻	$C_{33}H_{40}O_{20}$	756.2114	755.2042	13.338
35	*O*-Feruloylquinic acid	[M-H]⁻	$C_{17}H_{20}O_9$	368.1108	367.1037	13.729
36	Catechin-ol-*O*-*β*-D-hexopyranoside	[M-H]⁻	$C_{21}H_{22}O_{12}$	468.1269	467.1197	14.222
37	Kaempferol -deoxyhexose -pentose	[M-H]⁻	$C_{21}H_{24}O_{12}$	564.1481	563.1407	14.646
38	Kaempferol -rutinoside- deoxyhexose	[M-H]⁻	$C_{33}H_{40}O_{19}$	740.2168	739.2088	15.122
39	Salicylic acid	[M-H]⁻	$C_7H_6O_3$	138.0318	137.0245	15.348
40	Quercetin-dideoxyhexose	[M-H]⁻	$C_{27}H_{30}O_{15}$	594.1584	593.1514	15.652
41	Trimethoxycoumarin	[M-H]⁻	$C_{12}H_{12}O_5$	236.0686	235.0614	16.053
42	*p*-Coumaroyl quinic acid	[M-H]⁻	$C_{16}H_{18}O_8$	398.1215	397.1143	16.055
43	Kaempferol-deoxyhexose-pentose	[M-H]⁻	$C_{26}H_{28}O_{14}$	610.1538	609.1467	16.526
44	Quercitrin	[M-H]⁻	$C_{21}H_{20}O_{11}$	448.1004	447.0932	18.987
45	Apigenin di-hexoside	[M-H]⁻	$C_{27}H_{30}O_{15}$	594.1586	593.1513	19.358
46	Kaempferol-deoxyhexose-pentose	[M-H]⁻	$C_{26}H_{28}O_{14}$	624.1693	623.1622	19.876
47	Apigenin hexose	[M-H]⁻	$C_{21}H_{20}O_{10}$	432.1056	431.0984	21.439
48	Pentahydroxyisoflavone	[M-H]⁻	$C_{15}H_{10}O7$	302.0427	301.0355	22.023
49	Neocuscutoside isomer 1	[M-H]⁻	$C_{32}H_{38}O_{17}$	694.2112	693.2041	22.813
50	Neocuscutoside isomer 2	[M-H]⁻	$C_{32}H_{38}O_{17}$	694.2115	693.2038	22.943
51	Neocuscutoside isomer 3	[M-H]⁻	$C_{32}H_{38}O_{17}$	694.2113	693.1026	24.295
52	Linoside	[M-H]⁻	$C_{30}H_{36}O_{15}$	678.216	677.2092	25.146
53	Kaempferol -(p-coumarylhexose)	[M-H]⁻	$C_{27}H_{30}O_{15}$	594.1376	593.1304	25.16
54	Quercetin -(-di-p-coumarylhexose)	[M-H]⁻	$C_{39}H_{32}O_{16}$	756.1691	755.1621	26.129
55	9,10,18-TriHOME	[M-H]⁻	$C_{18}H_{34}O_5$	330.2408	329.2337	26.35
Positive ionization mode						
1	N,N,N-Trimethyllysine	[M+H]+	$C_9H_{21}N_2O_2^+$	188.1526	189.1603	1.198
2	N-hexosyl-L-asparagine	[M+H]+	C10H18N2O8	294.1064	295.1189	1.286
3	D-Mannitol	[M+H]+	$C_6H_{14}O_6$	182.0791	183.1391	1.301
4	N-(1-Deoxy-1- hexosyl)proline	[M+H]+	$C_{11}H_{19}NO_7$	277.1165	278.1235	1.382
5	L-Valine	[M+H]+	$C_5H_{11}NO_2$	117.0792	118.0662	1.6
6	N-(1-Deoxy-1- hexosyl)valine	[M+H]+	$C_{11}H_{21}NO_7$	279.1325	280.1393	1.653
7	D-Picolinic acid	[M+H]+	$C_6H_5NO_2$	123.032	124.0393	1.769
8	*p*-Coumaric acid	[M+H]+	$C_9H_8O_3$	181.074		2.245
9	Amino acid	[M+H]+	$C1_0H_{13}N_5O_4$	267.0969	268.1042	2.389
10	N-(1-Deoxy-1- hexosyl)leucine	[M+H]+	$C_{12}H_{23}NO_7$	293.148	294.1549	2.519
11	D-Phenylalanine	[M+H]+	$C_9H_{11}NO_2$	165.0793	166.0863	4.113
12	Quinacetol	[M+H]+	$C_{11}H_9NO$	187.0634	189.0724	6.869
13	*p*-Coumaroyl quinic acid	[M+H]+	$C_{16}H_{18}O_8$	338.1002	339.2103	10.409
14	Quercetin-[deoxyhexosyl-(1–2)-deoxyhexosyl-(1–6)-hexoside]	[M+H]+	$C_{33}H_{40}O_{20}$	756.2113	757.3193	13.332
15	*O*-Feruloylquinic acid	[M+H]+	$C_{17}H_{20}O_9$	390.0926	391.0999	13.718
16	Kaempferol-*O*-hexoside	[M+H]+	$C_{21}H_{20}O_{11}$	448.1005		15.105

(*continued on next page*)

Table 2 (*continued*)

N°	Compound	ESI	Formula	Mass	m/z	Retention Time
17	Kaempferol-(hexose-deoxyhexose)-deoxyhexose	[M+H]+	$C_{33}H_{40}O_{19}$	740.2168	741.2241	15.112
18	Piperic acid	[M+H]+	$C_{12}H_{10}O_4$	218.0581	219.0653	16.039
19	Trimethoxycoumarin	[M+H]+	$C_{12}H_{12}O_5$	236.0685	237.0894	16.039
20	Kaempferol-deoxyhexose-pentose	[M+H]+	$C_{26}H_{28}O_{14}$	610.1536	611.1611	16.526
21	Quercitin	[M+H]+	$C_{21}H_{20}O_{11}$	448.1006	449.1108	18.986
22	Apigenin di-hexoside	[M+H]+	$C_{27}H_{30}O_{15}$	594.1586	595.1659	19.356
23	Kaempferol-deoxyhexose-pentose	[M+H]+	$C_{26}H_{28}O_{14}$	624.1692	625.1769	19.87
24	Unknown m/z 246	[M+H]+		246.1256	247.0966	20.012
25	Pentahydroxyisoflavone	[M+H]+	$C_{15}H_{10}O_7$	302.0427	303.0501	22.025
26	Neocuscutoside isomer 1	[M+H]+	$C_{32}H_{38}O_{17}$	694.2115	695.2187	22.937
27	Neocuscutoside isomer 2	[M+H]+	$C_{32}H_{38}O_{17}$	694.2115	695.2187	24.293
28	Neocuscutoside isomer 3	[M+H]+	$C_{32}H_{38}O_{17}$	694.2113	695.2185	25.295

Table 3
Antioxidant properties of the tested extracts[a].

Extracts	DPPH (mg TE/g)	ABTS (mg TE/g)	CUPRAC (mg TE/g)	FRAP (mg TE/g)	Chelating (mg EDTAE/g)	PBD (mmol TE/g)
Ethyl acetate	17.84 ± 0.18^{c}	37.11 ± 1.65^{d}	61.98 ± 0.54^{c}	35.21 ± 0.11^{c}	14.27 ± 0.38^{ab}	1.86 ± 0.05^{a}
Ethanol	42.64 ± 1.24^{b}	54.69 ± 1.95^{c}	91.30 ± 1.09^{a}	57.69 ± 0.04^{a}	3.97 ± 0.53^{c}	1.28 ± 0.02^{b}
Ethanol/Water (70%)	50.58 ± 1.84^{a}	68.88 ± 3.03^{b}	74.32 ± 0.99^{b}	50.19 ± 0.62^{b}	13.98 ± 0.79^{b}	0.59 ± 0.02^{c}
Water (infused)	50.25 ± 1.25^{a}	80.06 ± 0.55^{a}	62.33 ± 1.61^{c}	50.05 ± 0.81^{b}	15.64 ± 0.26^{a}	0.68 ± 0.08^{c}

[a] Values are reported as mean ± SD of three parallel measurements. ABTS: 2,2′-azino-bis(3-ethylbenzothiazoline-6-sulphonic acid; DPPH: 1,1-diphenyl-2-picrylhydrazyl; CUPRAC: Cupric reducing antioxidant capacity; FRAP: Ferric reducing antioxidant power; PBD: Phosphomolybdenum; TE: Trolox Equivalent; EDTAE: EDTA equivalent. Different letters indicate significant differences between the tested extracts ($p < 0.05$).

Table 4
Enzyme inhibitory properties of the tested extracts[a].

Extracts	AChE (mg GALAE/g)	BChE (mg GALAE/g)	Tyrosinase (mg KAE/g)	Amylase (mmol ACAE/g)	Glucosidase (mmol ACAE/g)
Ethyl acetate	1.62 ± 0.06^{c}	3.41 ± 0.14^{a}	94.47 ± 3.03^{a}	0.71 ± 0.01^{a}	0.26 ± 0.01^{c}
Ethanol	2.28 ± 0.02^{a}	0.98 ± 0.16^{b}	63.36 ± 0.31^{b}	0.50 ± 0.01^{b}	1.03 ± 0.02^{a}
Ethanol/Water (70%)	2.00 ± 0.02^{b}	0.17 ± 0.01^{c}	45.21 ± 1.15^{c}	0.32 ± 0.01^{c}	0.88 ± 0.02^{b}
Water (infused)	1.00 ± 0.06^{d}	na	na	0.06 ± 0.01^{d}	0.29 ± 0.01^{c}

[a] Values are reported as mean ± SD of three parallel measurements. AChE: acetylcholinesterase; BChE: butyrylcholinesterase; GALAE: Galantamine equivalent; KAE: Kojic acid equivalent; ACAE: Acarbose equivalent; na: not active. Different letters indicate significant differences between the tested extracts ($p < 0.05$).

carbohydrates, sugar alcohol and amino acids. Most polyphenolic compounds and flavonoids better extract to ethyl acetate, while amino acid and carbohydrates to ethanol and water solvents.

3.3. Antioxidant activity

The antioxidant activity of various *T. apulum* aerial parts extracts was comprehensively evaluated using several assays, including DPPH, ABTS, CUPRAC, FRAP, chelating activity, and PBD, result illustrate in Table 3. The ethyl acetate extract exhibited moderate antioxidant properties, with DPPH, ABTS, CUPRAC, and FRAP values of 17.84 mg TE/g, 37.11 mg TE/g, 61.98 mg TE/g, and 35.21 mg TE/g, respectively. It also showed a chelating activity of 14.27 mg EDTAE/g and PBD of 1.86 mmol TE/g. The ethanol extract demonstrated significantly higher antioxidant activity, particularly in CUPRAC assay and FRAP assays measuring 91.30 mg TE/g and 57.69 mg TE/g, respectively, followed by 70% ethanol extract exhibited 74.32 and 50.19, respectively. The water extract had the highest ABTS activity at 80.06 mg TE/g and MCA 15.64 mg TE/g and showed considerable DPPH (50.25 mg TE/g) and FRAP (50.05 mg TE/g) values. These results indicate that different solvents can extract varying levels of antioxidants from *T. apulum* materials, with the ethanol and water extracts generally showing superior antioxidant activities. Given that *T. apulum* is widely regarded as possessing substantial antioxidant capacity (Pieroni et al., 2002; Savo et al., 2019), the elevated antioxidant values observed in nearly all tested assays further corroborate their strong antioxidant potential. In the previous study, extracts and essential oil of *T. apulum* demonstrated notable antioxidant activity (Maresca et al., 2024; Pieroni et al., 2002). Matejić et al. investigated the water extract of *T. maximum* exhibited a higher free radical scavenging activity with an IC50 value of 4.042 mg/mL compared to the methanol extract, which had an IC50 value of 7.825 mg/mL (MatejiÄ et al., 2013). The results of the PBD assay for the tested extracts did not correlate with the radical scavenging activity, reducing power assays, or TPC and TFC. For example, ethyl acetate extracts exhibited lower antioxidant activity in all five tested antioxidant assays and TFC compared to the other extracts, yet showed higher PBD antioxidant activity 1.86 mmol TE/g. In contrast, water and 70% ethanol extracts demonstrated higher TPC and TFC but lower PBD assay activity, 0.68 86 mmol TE/g and 0.5986 mmol TE/g, respectively, that due to the varying mechanisms of each assay.

Table 5
The inhibition (IC_{50} (μg/mL) of human carbonic anhydrase isoenzymes I and II (hCA I and hCA II).

Extracts	IC_{50} (μg/mL)			
	hCA I	r^2	hCA II	r^2
Ethyl acetate	3.871	0.9378	15.065	0.9223
Ethanol	19.25	0.9051	1.048	0.9723
Ethanol/Water	138.6	0.9195	1.174	0.9072
Water	7.451	0.9486	9.00	0.9034
Asetazolamid	0.154	0.985	0.289	0.9514

3.4. Enzyme inhibition activity

The enzyme inhibition activities of various *T. apulum* aerial parts extracts were investigated, revealing distinct inhibitory effects on several enzymes, results show in Table 4. The ethyl acetate extract demonstrated significant inhibition, with values of 1.62 mg GALAE/g for AChE, 3.41 mg GALAE/g for BChE, 94.47 mg KAE/g for tyrosinase,

Table 6
Minimal Inhibitory Concentration of *T. apulum* extracts. Results are expressed in μg/mL and are the average (±SD) of three independent experiments. As control, we used tetracycline 7 μg/mL a: $p < 0.5$; b: $p < 0.1$; ns: not significative (ANOVA followed by Dunnett's multiple comparison test).

Extracts/Standard	*A. baumanii*	*E. coli*	*L. monocytogenes*	*P. aeruginosa*	*S. aureus*
Ethyl-acetate	40 (±2.0)[a]	>50[b]	38 (±1.0)[a]	>50[b]	>50[b]
Ethanol	>50[b]	40 (±2.0)[a]	38(±2.0)[a]	>50[b]	>50[b]
Ethanol/water (70%)	>50[b]	38(±2.0)[a]	38(±2.0)[a]	38 (±2.0)[a]	40 (±1.0)[a]
Water (infused)	>50[b]	38(±1.0)[a]	38 (±1.0)[a]	36 (±1.0)[nd]	>50[b]
Tetracycline	30.0 (±1.0)	30.0(±2.0)	30.0 (±1.0)	32.0(±1.0)	34.0(±2.0)

Table 7
Biofilm inhibitory activity (expressed as percentage) of the ethyl acetate, ethanol, ethanol-water extracts and water infuse of *T. apulum* against the pathogens *Acinetobacter baumannii*, *Escherichia coli*, *Listeria monocytogenes*, *Pseudomonas aeruginosa*, and *Staphylococcus aureus*. The extract was tested at 10 μg/mL (10) and 20 μg/mL (20). The data represent the average of three independent experiments (±SD) a: $p < 0.5$; b: $p < 0.01$; ns: not significative (ANOVA followed by Dunnett's multiple comparison test).

CV	Ethyl-acetate-10	Ethyl-acetate- 20	Ethanol-10	Ethanol-20	Ethanol-water-10	Ethanol-water-20	Water (infuse)-10	Water (infuse)-20
A baumannii	14.12 [a] (±0.11)	23.87 [a] (±1.99)	0.00 (±0.00)	0.00 (±0.00)	0.00 (±0.00)	0.00 (±0.00)	0.00 (±0.00)	0.00 (±0.00)
E coli	0.00 (±0.00)	0.00 (±0.00)	0.00 (±0.00)	0.00 (±0.00)	24.84 [a] (±1.34)	49.93 [c] (±3.47)	41.76 [b] (±1.02)	45.22 [b] (±0.54)
L monocytogenes	0.00 (±0.00)	26.84 [a] (±2.13)	0.00 (±0.00)	0.00 (±0.00)	25.06 [a] (±1.67)	28.16 [b] (±1.13)	3.06 [ns] (±0.23)	35.30 [b] (±3.02)
P aeruginosa	0.00 (±0.00)	0,00 (±0.00)	0.00 (±0.00)	0.09 (±0.02)	39.49 [b] (±2.65)	50.68 [c] (±2.44)	41.45 [b] (±3.01)	44.46 [b] (±2.87)
S aureus	0.00 (±0.00)	2.67 [ns] (±0.04)	0.00 (±0.00)	21.56 [a] (±1.87)	0.00 (±0.00)	29.43 [b] (±2.45)	0.00 (±0.00)	0.00 (±0.00)

0.71 mmol ACAE/g for α-amylase, and 0.26 mmol ACAE/g for α-glucosidase.

Over 55 million people worldwide suffer from Alzheimer's disease (AD), with its prevalence growing as the population ages (Gonçalves-Pereira et al., 2021). Current treatments often target the cholinergic hypothesis, which links AD symptoms to the breakdown of cholinergic neurons and acetylcholine (ACh) by cholinesterase (Hampel et al., 2018). Inhibiting the brain's acetylcholinesterase (AChE) and butyrylcholinesterase (BChE) enzymes helps improve cognitive function by preventing ACh degradation (Giacobini, 2003; Tan et al., 2014). The ethanol extract exhibited the highest inhibition of AChE at 2.28 mg GALAE/g, closely followed by the 70% ethanol extract at 2.00 mg GALAE/g, indicating a neuroprotective effect (Giacobini, 2003; Tan et al., 2014). In contrast, the ethyl acetate extract demonstrated greater anti-BChE activity at 3.41 mg GALAE/g, showing anti-AD activity (Tan et al., 2014). This extract also showed higher anti-tyrosinase activity at 94.47 mg KAE/g, suggesting its role in skin protective effect (Rescigno et al., 2002). In the study conducted by Orhan et al. it was found that methanol extracts of *T. apulum* demonstrated significant inhibitory effects on three key enzymes: ACHE, BCHE, and tyrosinase (Orhan et al., 2016). The potential enzyme inhibitory activity observed in the study may be attributed to the presence of coumarin derivatives. Previous research has indicated that both coumarin derivatives and coumarin-rich plants exhibit significant inhibitory effects on AChE, BChE, and tyrosinase (Gardelly et al., 2021; Orhan et al., 2016, 2021). This evidence provided a strong rationale for conducting the current study, which aims to further explore and confirm the inhibitory potential of these compounds. On another hand, the water extract showed no inhibition of BChE and tyrosinase. Concerning the carbohydrase enzymes, α-amylase and α-glucosidase (Aakko et al., 2020), all the tested extracts showed lower inhibition, except for the ethanol extract which notably inhibited glucosidase 1.03 mmol ACAE/g. These findings highlighted the varying degrees of enzyme inhibition by different *T. apulum* extracts, suggesting potential applications in managing enzyme-related disorders.

3.5. Inhibition of human carbonic anhydrase isoenzymes I and II

Carbonic anhydrase (CA) enzymes are present in all living systems and play roles in various physiological and pathological processes, including pH regulation, carboxylation reactions, fluid balance, neurological disorders, osteoporosis, tumorigenicity (Akıncıoğlu et al., 2014; Gülçin et al., 2004; Supuran & Scozzafava, 2007). These isoenzyme efficiently convert carbon dioxide to bicarbonate and are crucial for several biological functions (Hassan et al., 2013). Inhibitors of CA activity have been used therapeutically for decades to treat conditions such as high blood pressure, hypoglycemia, and cancer (Nar et al., 2013).

Table 5 provided detailed the inhibitory effects of different extracts of aerial parts of examined included ethyl acetate, ethanol, 70% ethanol, and water from the aerial parts of *T. apulum* on the enzymes hCA I and hCA II. Each extract was tested to determine its IC_{50} values, which indicate the concentration required to inhibit the enzyme activity by 50%. For hCA I, the ethyl acetate extract showed an IC_{50} value of 3.871 μg/mL with a correlation coefficient (r^2) of 0.9378, demonstrated higher inhibition activity. In contract the 70% ethanol extract had lower inhibition activity given the IC_{50} value of 138.6 μg/mL and an r^2 of 0.9195. In the case of hCA II, the ethanol extract was the most potent among the plant extracts, with an IC_{50} value of 1.048 μg/mL followed by 70% ethanol extract showed a slightly higher IC_{50} value of 1.174 μg/mL. The ethyl acetate extract demonstrated a lower hCA II inhibition activity with the IC_{50} value of 15.065 μg/m. The standard inhibitor acetazolamide remained the most potent inhibitor for both enzymes across all extracts tested. No studies have been conducted thus far to investigate the effects of *T. apulum* extracts on hCA I and hCA II. Consequently, this study represents the initial exploration of these effects. The inhibition of hCA I and hCA II by *T. apulum* aerial parts extracts indicate the potential of this plant extracts in the development of therapeutic agents for conditions associated with these enzymes.

3.6. Antibiofilm activity

Plants belonging to the *Tordylium* genus have generally demonstrated antibacterial efficacy and, to our knowledge, there are not many works focused on the antibiofilm activity exhibited by *T. apulum* according to the extraction methodology applied. Extracts of *T. maximum*, for example, have shown antibacterial capacity against *E. coli*, *L. monocytogenes*, *S. aureus*, *P. aeruginosa* (MatejiÄ et al., 2013). The antibacterial activity of *T. aegyptiacum* L extract was evaluated *vs. L. monocytogenes*, and *S. aureus* (Christou et al., 2024). To our knowledge, it is the first time that different types of *T. apulum* extracts have been tested to verify their potential antibiofilm action against *A. baumanni*. Indeed, it is undoubtedly the first time that the possible ability of these extracts to inhibit the sessile cell metabolism of the five pathogens and

Table 8
Inhibitory activity (expressed as percentage) of the ethyl acetate, ethanol, ethanol-water extracts and water infuse of *T. apulum* against the metabolism of the sessile cells of *Acinetobacter baumannii*, *Escherichia coli*, *Listeria monocytogenes*, *Pseudomonas aeruginosa*, and *Staphylococcus aureus*. The honey was tested at 10 mg/mL (_10) and 20 mg/mL (_20). The data represent the average of three independent experiments (±SD) a: $p < 0.5$; b: $p < 0.01$; c: $p < 0.001$; ns: not significative (ANOVA followed by Dunnett's multiple comparison test).

MTT	Ethyl-acetate_ 10	Ethyl-acetate_ 20	Ethanol_ 10	Ethanol_ 20	Ethanol-water_10	Ethanol-water_20	Water (infuse) _10	Water (infuse) _20
A baumannii	0.00 (±0.00)	0.00 (±0.00)	0.00 (±0.00)	0.34 ^{ns} (±0.05)	0.00 (±0.00)	5.46 ^{a} (±0.12)	0.00 (±0.00)	6.65 ^{a} (±0.25)
E coli	0.00 (±0.00)	0.00 (±0.00)	12.65 ^{a} (±1.05)	13.51 ^{a} (±0.98)	35.60 ^{b} (±2.25)	50.01 ^{c} (±4.45)	32.74 ^{b} (±2.54)	39.95 ^{b} (±3.15)
L monocytogenes	4.97 ^{a} (±0.85)	35.46 ^{b} (±2.21)	6.48 ^{a} (±0.23)	7.54 ^{a} (±0.31)	0.00 (±0.00)	24.84 ^{a} (±2.12)	9.59 ^{a} (±0.77)	39.10 ^{b} (±2.29)
P aeruginosa	35.32 ^{b} (±2.17)	40.03 ^{b} (±3.34)	14.72 ^{a} (±1.09)	35.81 ^{b} (±3.09)	22.87 ^{a} (±1.13)	42.78 ^{b} (±2.98)	52.22 ^{c} (±3.34)	62.11 ^{c} (±4.12)
S aureus	33.78 ^{b} (±2.31)	40.82 ^{b} (±2.67)	0.00 (±0.00)	15.40 ^{a} (±1.12)	18.64 ^{a} (±1.33)	62.60 ^{c} (±3.31)	50.52 ^{c} (±2.65)	61.94 ^{c} (±1.76)

Table 9
Cytotoxic effects of the tested extracts on cancer and normal cell lines (IC_{50}).

	HELA	A549	DU-145	MDA-MB-231	HUVEC
Ethyl acetate	75.94	71.56	100.45	78.09	68.93
Ethanol	61.56	69.6	98.67	101.54	115.9
Ethanol/Water	59.57	48.58	76.89	56.31	89.25
Water	33.47	41.48	45.76	53.71	115.5

thus somehow limit the changes that lead to an increase in their virulence. We performed the tests using five pathogenic strains, *A. baumannii*, *E. coli*, *L. monocytogenes*, *P. aeruginosa*, and *S. aureus* MRSA. All of them, except *L. monocytogenes*, have been included by the WHO in the list of critical (*A. baumanni and E. coli*) and highly hazardous (*P. aeruginosa and S. aureus*) (Organization, 2007). We thought we would carry out the tests also vs. *L. monocytogenes* because this bacterium, despite not being present in the WHO list, is still capable of causing severe poisoning if present as a contaminating agent on foods (Osek & Wieczorek, 2022). Table 6 shows the results of MIC test, compulsory to carry the crystal violet and MTT test, which results are shown in Tables 7 and 8, respectively.

The ethyl-acetate extract showed weak antibiofilm activity in crystal violet. Through such test, we saw that the most sensitive strains were *A. baumannii* (23.87%) and *L. monocytogenes* (26.84%). On the contrary, the ethanol-water extract and water infuse acted on the biofilm of *E. coli* (49.93% and 45.22%, respectively), and the biofilm of *P. aeruginosa* (50.68% and 44.46%, respectively). Using ethanol and in ethanol-water extracts also determined an inhibitory biofilm action on *S. aureus* (21.56% and 29.43%), which was utterly insensitive to the water extract and showed a very weak sensitivity to ethyl acetate extract. The action of the various extracts on the metabolism of the cells of the five pathogens only partially confirmed the results obtained from the crystal violet test, meaning that, in some cases, the inhibitory action of the extracts was not only focused on blocking cellular metabolism. Thus, the ethyl acetate extract confirmed its inhibitory action on the metabolism of the sessile cells of *L. monocytogenes* (35%–46%). Such extract, ineffective against the biofilm of *P. aeruginosa* and *S. aureus*, nevertheless managed to inhibit the metabolism of their sessile cells, thus limiting

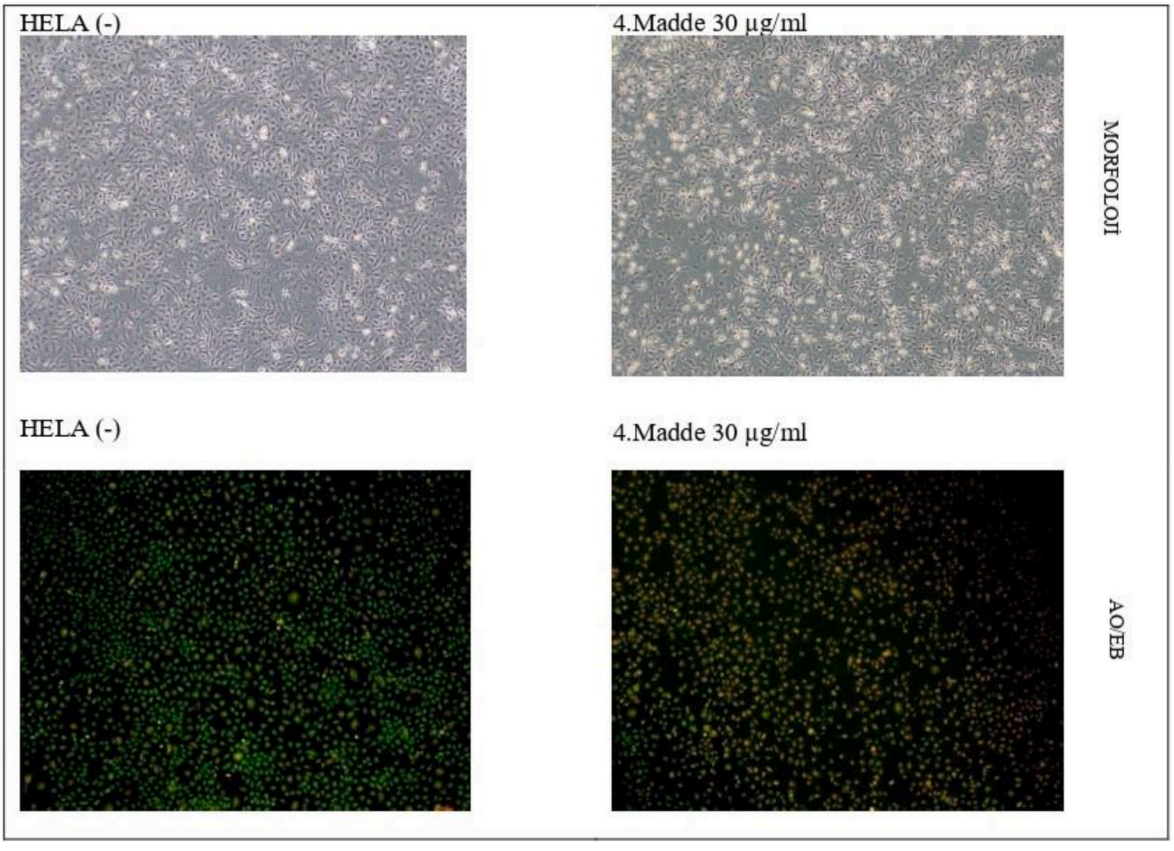

Fig. 1. AO/EB staining after water extract (30 µg/mL) applied to HELA cell.

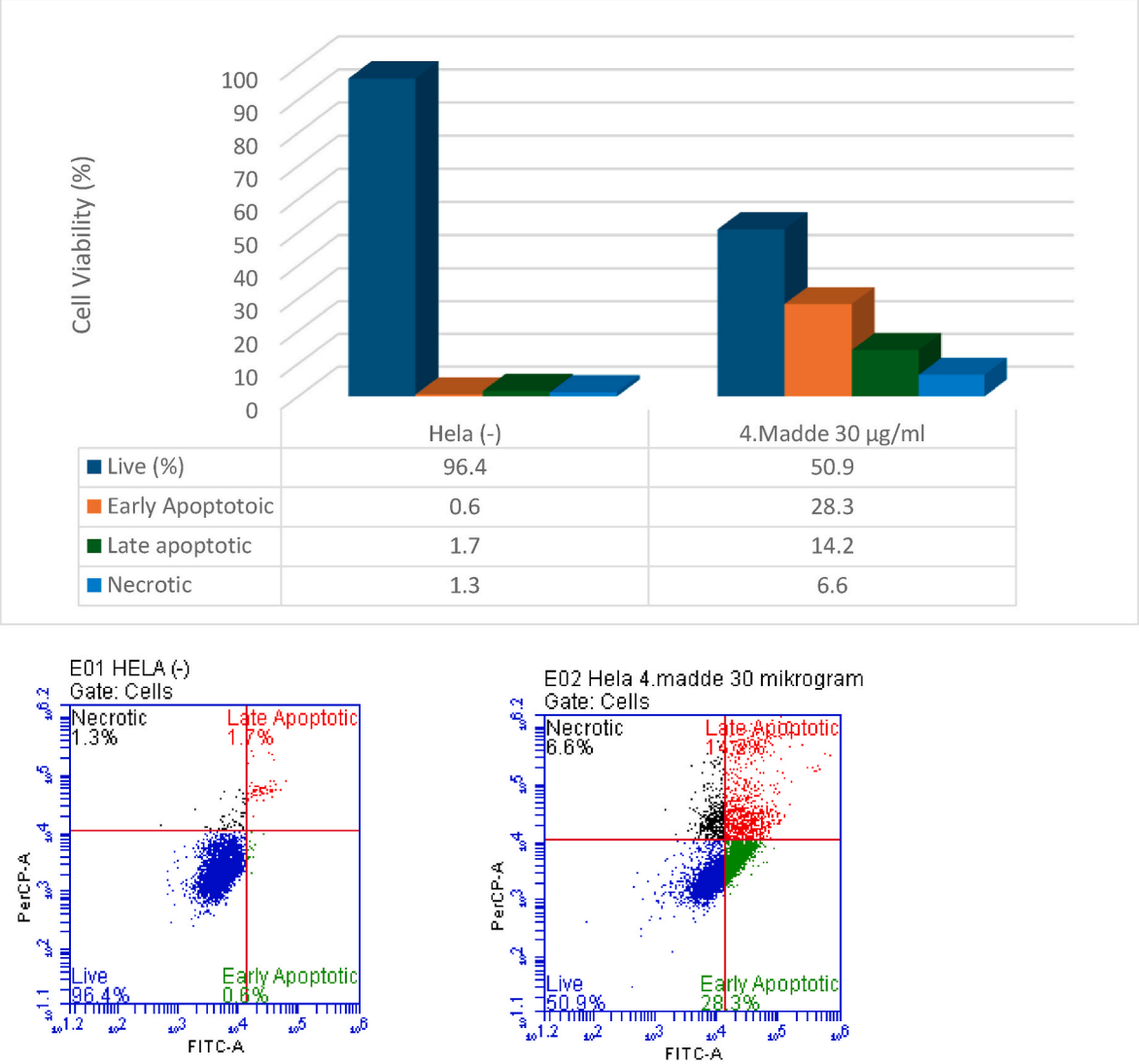

Fig. 2. Annexin-V/PI staining results after applying water (30 µg/mL) to HELA cell. Blue: Live-[(FITC-)/(PI-)]; Green: Early apoptotic [(FITC+)/(PI-)]; Red: Late apoptotic [(FITC+)/(PI+)]; Black: Shows necrotic [(FITC+)/(PI+)] cells. (For interpretation of the references to color in this figure legend, the reader is referred to the Web version of this article.)

Table 10
The binding energy of the bioactive compounds in *T. apulum* against some selected target proteins.

Compound	AChE	BChE	Tyrosinase	Amylase	Glucosidase	BCL-2	CDK2	TRAF2
O-Feruloylquinic acid	−9.21	−5.51	−5.15	−8.01	−5.64	−6	−8.45	−10.13
Kaempferol 3-rutinoside-7-rhamnoside	−13.02	−14.01	−10.13	−11.1	−6.83	−7.31	−9.81	−12.16
O-Coumaroylquinic acid	−5.03	−9.31	−7.12	−8.78	−7.23	−7.22	−7.45	−12.06
Apigenin diglucoside	−15.01	−10.44	−7.81	−10	−5.89	−6.09	−7.98	−11.13
Neocuscutoside C.	−11.14	−11.09	−6.86	NA	−5.44	−6.07	−9.57	−9.21

some of the mechanisms that lead to chemical changes inside their cells and their increased virulence. Ethanol-water and water extracts proved effective in inhibiting the metabolism of the sessile cells of almost all pathogenic strains except *A. baumannii*, which was poorly sensitive. The percentage of inhibition caused by the ethanol-water extract, ranged between 5.46% (vs.*A. baumannii*) to even 60%–62% (vs. *S. aureus*). This could imply that *S. aureus*, which was relatively insensitive to the action of the extracts, instead proved sensitive to the action of the extracts on the metabolism of its sessile cells. In the case of the water extract, we observed the same behavior. Once again, *A. baumannii* was the least sensitive strain (inhibition = 6.65%). *P. aeruginosa* (62.11%) and *S. aureus* (61.94%) were the most sensitive strains. In the latter case, therefore, the water extract, which was ineffective in blocking the biofilm of *S. aureus*, instead proved to be highly effective in blocking its metabolism.

3.7. Cytotoxic effects

Cancer is the biggest problem worldwide and therefore urgent precautions are needed to combat cancer. Synthetic drugs are still at the forefront of cancer treatment, but long-term use causes unpleasant side effects. In this sense, we must replace synthetic drugs with novel, effective and natural medicines (Zhang et al., 2024). In the last decade, several plants have been proposed as anticancer agents for medical

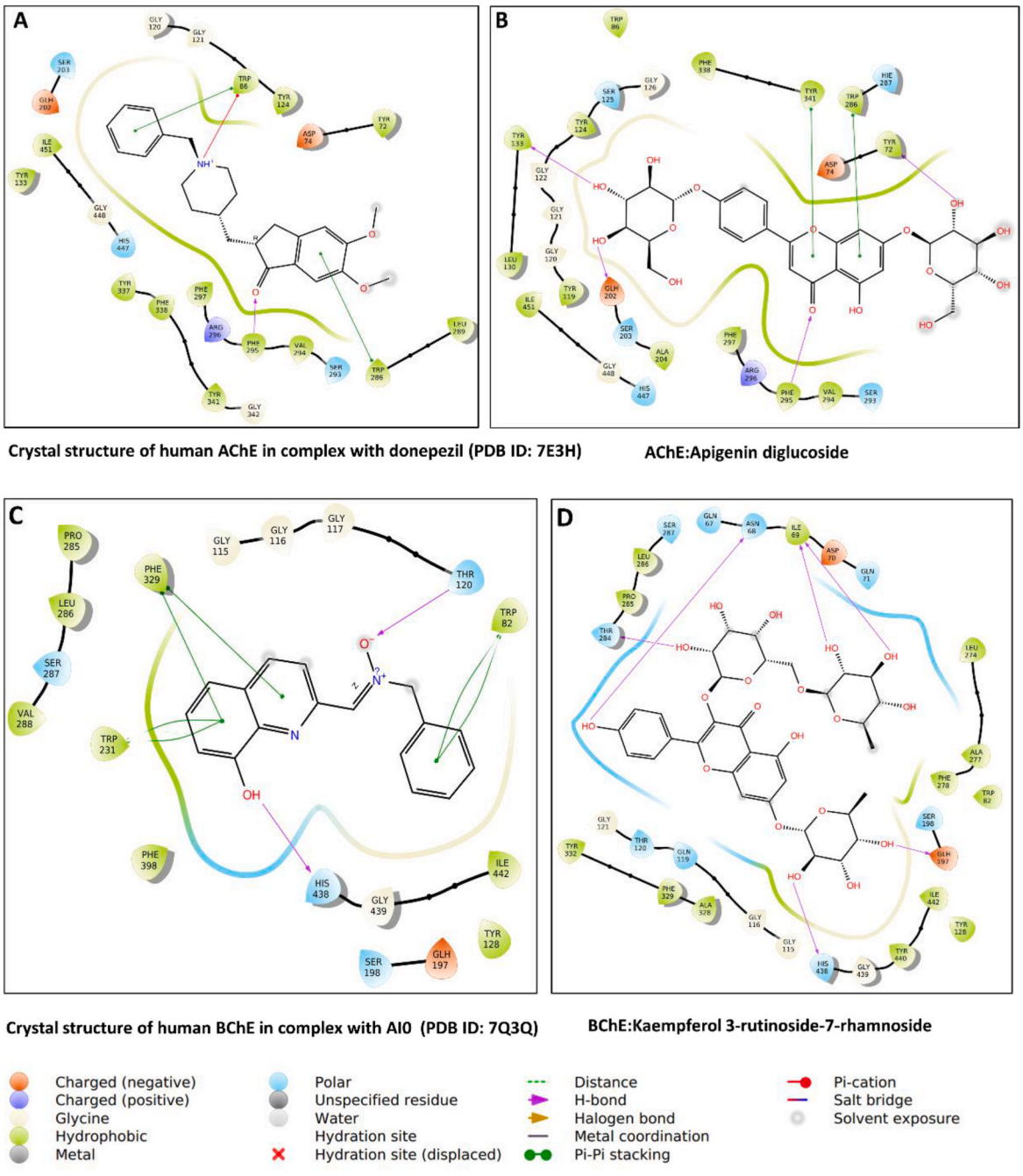

Fig. 3. Protein-ligand interaction: (A) crystal structure of human AChE in complex with donepezil (PDB ID: 7E3H), (B) docking complex of AChE with apigenin diglucoside, (C) crystal structure of human BChE in complex with AI0 (PDB ID: 7Q3Q), (D) docking complex of BChE with kaempferol 3-rutinoside-7-rhamnoside.

applications (Ayna et al., 2021; Kaplan, 2021; Yang et al., 2024). From this point on, we examined the cytotoxic effects of the test extracts on four cancer cell lines (HELA, A549, DU145 and MDA-MB-231) and one normal cell (HUVEC). The IC_{50} values are given in Table 9. Apparently, the tested extracts showed anti-cancer effects on the tested cell lines. In particular, the water extract was the most active on HELA with an IC_{50} value of 33.47 μg/mL. Additionally, the water extract didn't have as much of an effect on normal cells. Since the water extract had the strongest anticancer properties, we examined the apoptotic effect of this extract in further experiments. To detect cell death morphology, we performed AO/EB staining after 30 μg/mL water extract (30 μg/mL), the cell number decreased and they recorded with green-yellow color (Fig. 1). The apoptotic effect of the water extract was tested using Annexin VI/PI staining and the results are shown in Fig. 2. We found only a few studies in the literature on the cytotoxic effects of members of the genus *Tordylium*. In a previous study by Kofina et al. (Kofinas, Chinou, Loukis, Harvala, Roussakis, et al., 1998), seven coumarins isolated from *T. apulum* and tested on gill non-small cell carcinoma cell lines were examined, and all coumarins showed higher values with low IC_{50} (<20 μg/mL). In another study by Barthomeuf et al. (Barthomeuf et al., 2005), cnidiadine was isolated from *T. apulum* and the compound showed a significant effect on MDLK-MDR1 cell line. Overall, the coumarins can be attributed to the observed anticancer properties of the *Torydlium* genus. In our current study, we also noted the presence of some coumarins (Liqcoumarin, 5,6,7-Trimethoxycoumarin, and 4-Hydroxycoumarin, etc.) in the tested extracts. In addition to coumarins, we detected in the tested extracts the presence of some flavonoids (apigenin, kaempferol and quercitrin etc.) that may also contribute to

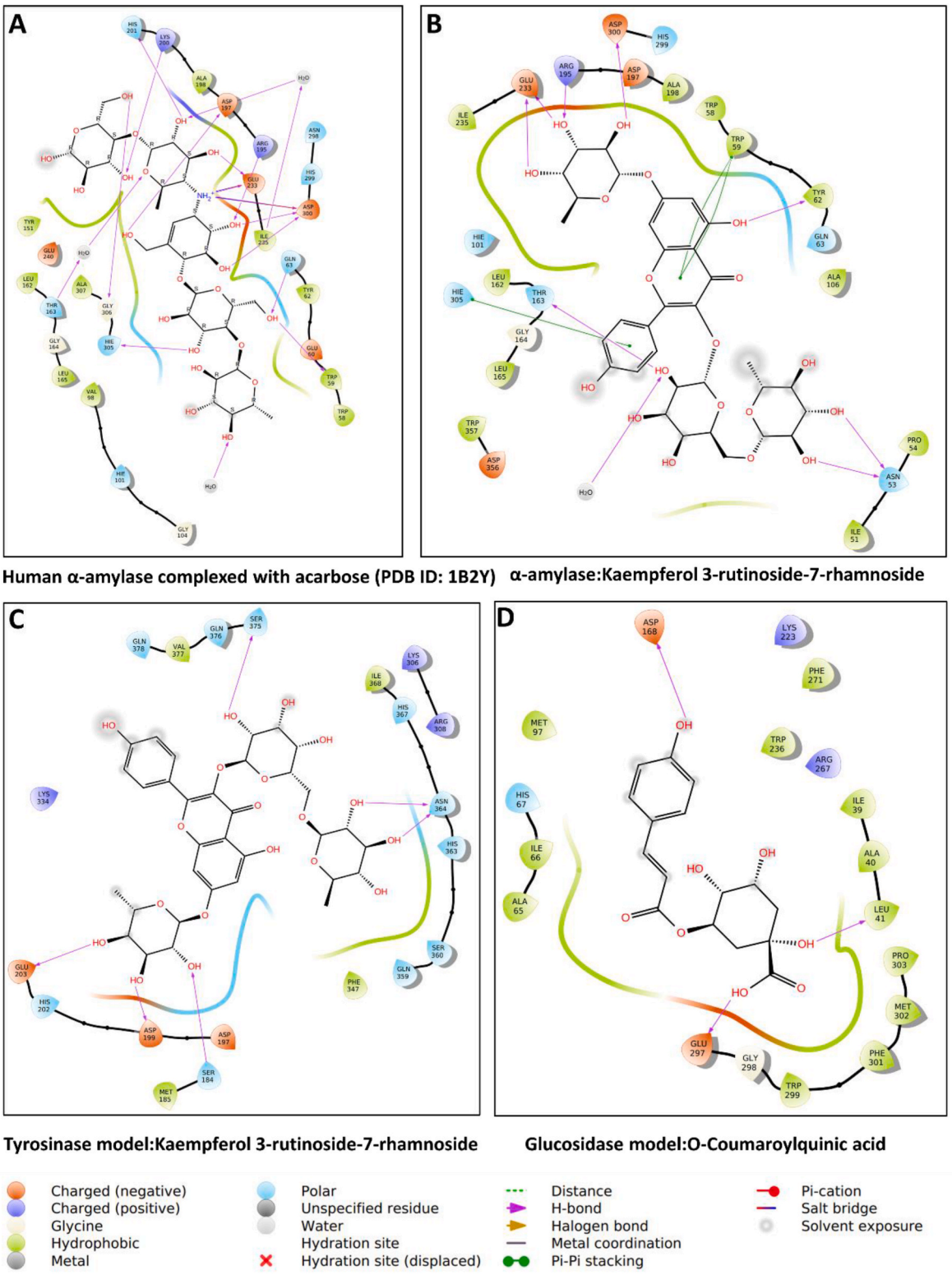

Fig. 4. Protein-ligand interaction: (A) crystal structure of α-amylase in complex with acarbose (PDB ID: 1B2Y), (B) docking complex of α-amylase with kaempferol 3-rutinoside-7-rhamnoside, (C) docking complex of the homology model of tyrosinase with kaempferol 3-rutinoside-7-rhamnoside, (D) docking complex of the homology model of glucosidase with O-Coumaroylquinic acid.

the anticancer effect, especially the apoptotic effect (Cincin et al., 2014; Fouzder et al., 2021; Yang et al., 2021). From this point, *T. apulum* can be considered as a source of natural anticancer compounds in chemotherapeutic applications.

3.8. Molecular modeling results

Table 10 shows the predicted binding energies for the bioactive chemicals in the extract of *T. apulum* against the studied target proteins. Apigenin diglucoside showed the highest binding propensity against

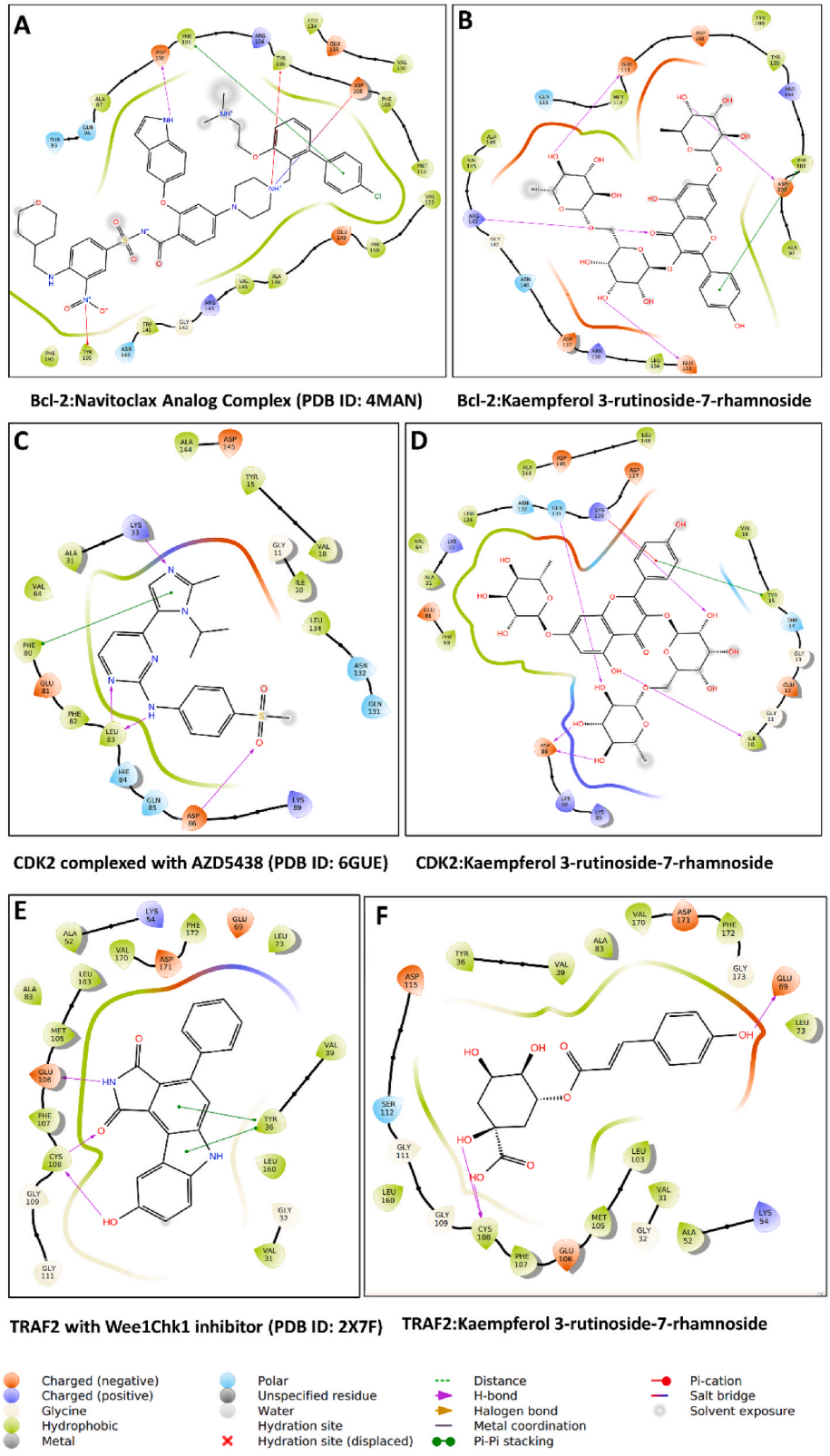

Fig. 5. Protein-ligand interaction: (A) crystal complex of Bcl-2 with navitoclax analog (PDB ID: 4MAN), (B) docking complex of Bcl-2 with kaempferol 3-rutinoside-7-rhamnoside, (C) crystal complex of CDK2/Cyclin A with AZD5438 (PDB ID: 6GUE), (D) docking complex of CDK2 with Kaempferol 3-rutinoside-7-rhamnoside, (E) crystal complex of TRAF2 with Wee1Chk1 inhibitor (PDB ID: 2 × 7F), and (F) docking complex of TRAF2 with kaempferol 3-rutinoside-7-rhamnoside.

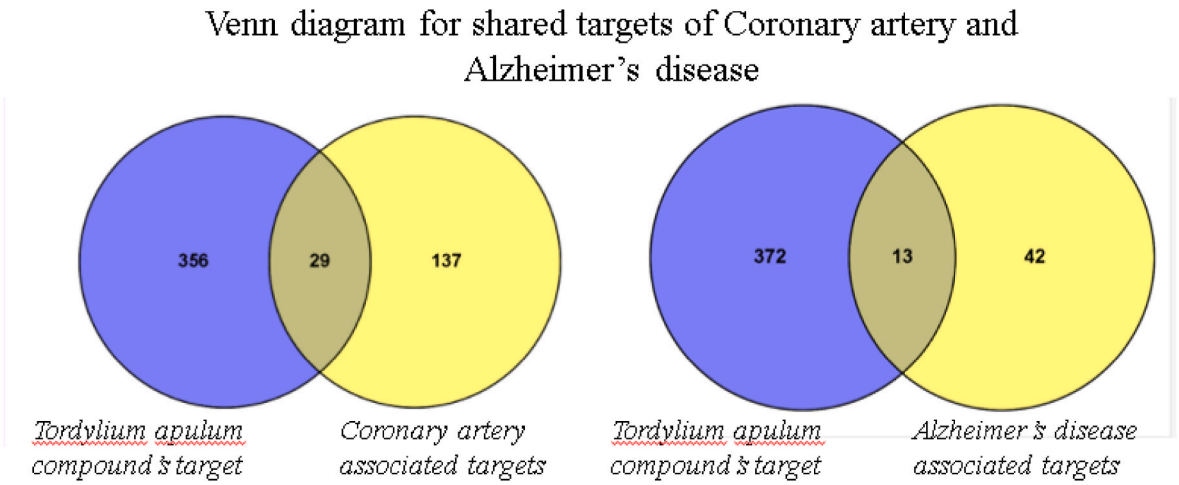

Fig. 6. Venn diagram illustrates overlapping of 141 targets associated with Coronary artery and 385 compound targets of *Tordylium apulum*, revealing shared set of 29 common targets and overlapping of 55 targets associated with Alzheimer's disease and 385- compound targets of *Tordylium apulum*, revealing shared set of 13 common targets.

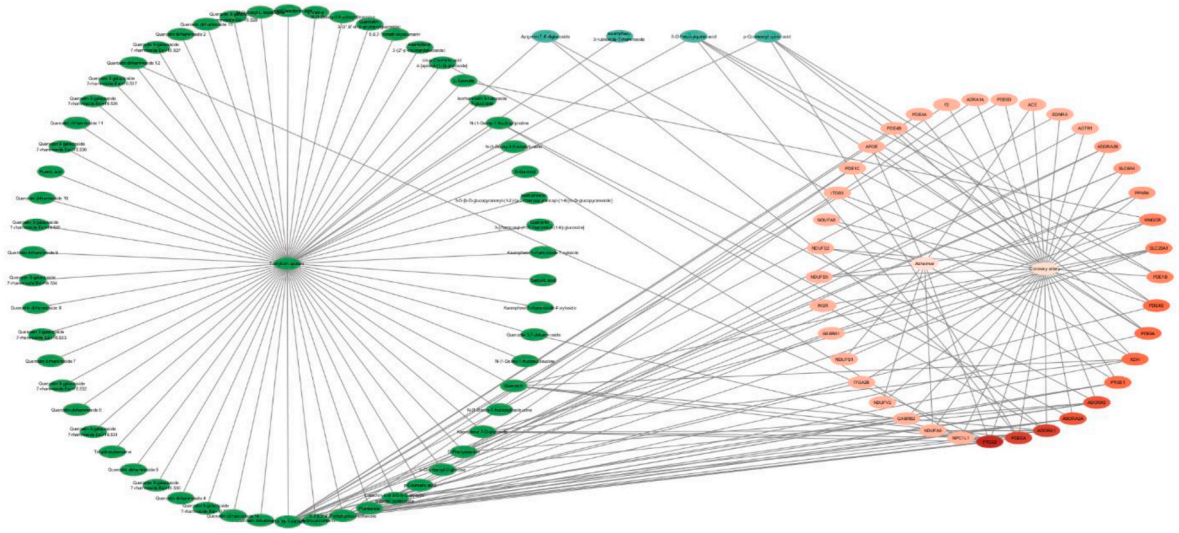

Fig. 7. Compound-target network construction of compound target and disease target between *Tordylium apulum* and coronary artery disease &Alzheimer's disease where green color nodes represent the compounds and red color represents the disease target nodes. (For interpretation of the references to color in this figure legend, the reader is referred to the Web version of this article.)

AChE while binding moderately to the rest of the proteins under study. Interestingly, kaempferol 3-rutinoside-7-rhamnoside appeared to have a pan-inhibition potential while other compounds demonstrated varied levels of binding strength to these proteins. For instance, compared to the crystal structure of AChE with donepezil (PDB ID: 7E3H) (Fig. 3A) (Dileep et al., 2022), Apigenin diglucoside was found to have the following common interactions with the amino acid residues in the active site of AChE: a H-bond with Phe295, π-π stacked interaction with Trp286, hydrophobic contacts with Tyr124, Val294, Phe297, and van der Waals interactions with Asp74, Ser293, Arg296, and His447. Other interacting residues found in the docking complex that were also present in the crystal structure include Tyr72 and Tyr133, which make H-bonds in the docking complex but hydrophobic contacts in the crystal complex (Fig. 3B). These interactions and the like suggest the potential of Apigenin diglucoside to inhibit the activity of AChE. Similarly, several interacting residues were found to be in common between the crystal structure of human BChE in complex with AI0 (PDB ID: 7Q3Q), (Fig. 3C) and its docking complex with kaempferol 3-rutinoside-7-rhamnoside, even though they were not necessarily of the same type. For instance, while Glu197 and Thr284 formed H-bonds with hydroxyl groups of kaempferol 3-rutinoside-7-rhamnoside, these residues formed van der Waals interactions with the crystal complex. Other interactions that enhanced the binding of the compound include H-bonds with Asn68 and Ile69, and multiple hydrophobic and van der Waals interactions all over the active site of the enzyme (Fig. 3D).

Also, a comparison between the crystal structure of α-amylase complexed with acarbose (a widely-used drug for the management of type 2 diabetes mellitus (Elks & Ganellin, 1990)) (PDB ID: 1B2Y) (Fig. 4A) (Nahoum et al., 2000), and the docking complex of α-amylase with kaempferol 3-rutinoside-7-rhamnoside identified important common interaction, which includes H-bonds with Thr163, Asp195, Glu233, Asp300. Other residues in the docking complex, which may not necessarily be involved in the same interaction as in the crystal complex, include but are not limited to Tyr62, Gln63, Ala198, His299, His305, and more—forming a variety of interactions that enhanced the binding of the ligand (Fig. 4B). The same ligand, kaempferol 3-rutinoside-7-rhamnoside, was found to exhibit strong binding to the homology model of tyrosinase, and these include H-bonds, via multiple hydroxyl

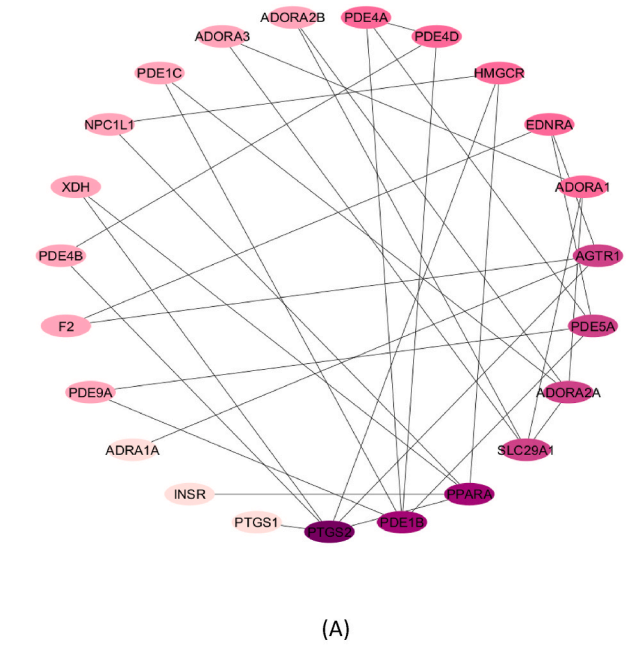

(A)

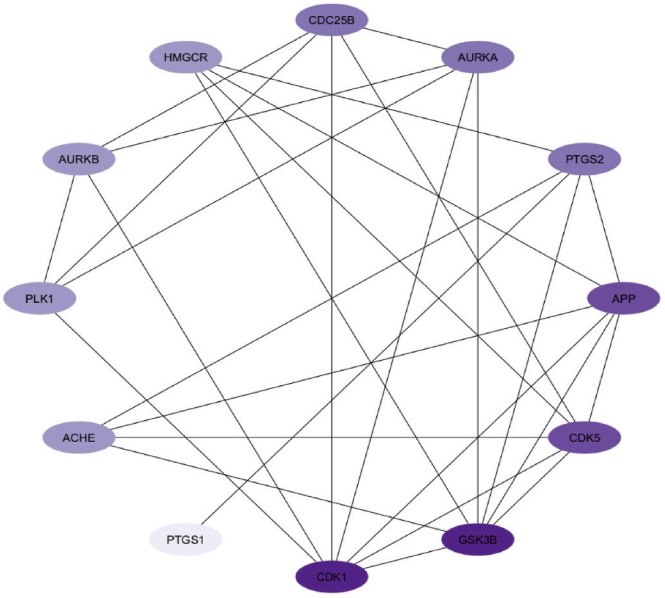

(B)

Fig. 8. (A) Protein-Protein interaction network, the color gradient depicts the no. Of edges a node has in the network, Hub genes of coronary artery's common target. (B) Protein-Protein interaction network, the color gradient depicts the no. Of edges a node has in the network, Hub genes of Alzheimer's disease common targets. (For interpretation of the references to color in this figure legend, the reader is referred to the Web version of this article.)

(A)

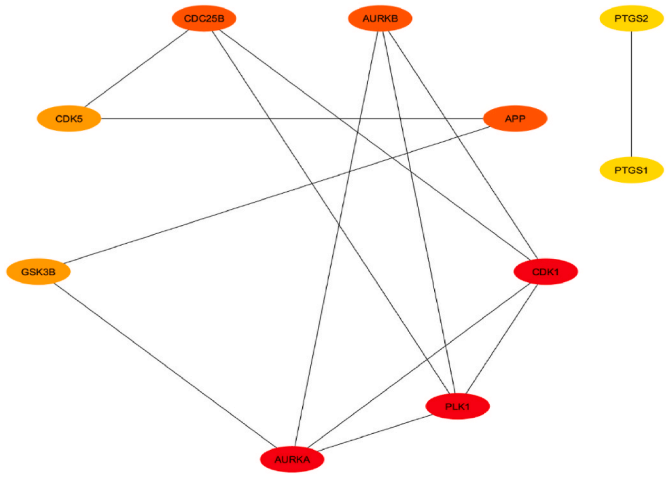

(B)

Fig. 9. (A) Top 10° node in Protein-Protein Interaction network Common targets between Coronary artery and *Tordylium apulum*. (B) Top 10° nodes in Protein-Protein Interaction network common targets between Alzhiemer's disease and *Tordylium apulum*.

groups, with Ser184, Asp199, Glu203 close to the entrance to the enzyme's active site tunnel; H-bonds with Asn364 and Ser375 deep inside. In addition, van der Waals interactions were formed with residues such as His202, Gln359, and Gln378, as well as hydrophobic interactions with Met185, Phe347, Ile368, and Val377 (Fig. 4C). Similarly, the interaction between O-Coumaroylquinic acid and the homology model of glucosidase was examined. This relatively smaller bioactive compound was completely buried in the catalytic site of glucosidase, forming H-bonds with the backbone of Leu41, and the sidechain of Asp168 and Glu297; several hydrophobic contacts with residues that include but are not limited to Ala40, Met97, and Trp299; as well as van der Waals interactions with His67, Lys223, and Arg267 (Fig. 4D).

Furthermore, the interaction of the cocrystal ligand, navitoclax analog, with Bcl-2 (PDB ID: 4MAN) (Fig. 5A) (Souers et al., 2013) was compared to that of kaempferol 3-rutinoside-7-rhamnoside with Bcl-2. Although several interacting residues were found to be in common between the crystal and docking complexes, the types of interactions were different in most cases. For example, Asp100 engaged in H-bond formation in both complexes, Glu133 and Arg143 formed H-bonds in the docking complex but engaged in van der Waals interaction in the crystal complex. Other common interactions that may be critical for binding include hydrophobic contact with Ala97, Val145, and Met112—among others, and van der Waals interactions with residues like Asp104 and Gln140, as well as π-π stacked interactions with Phe101 (Fig. 5B).

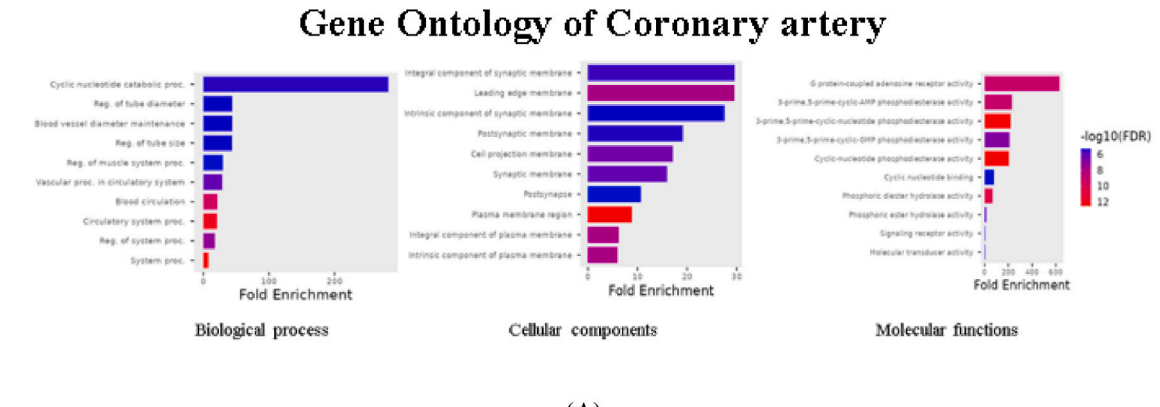

(A)

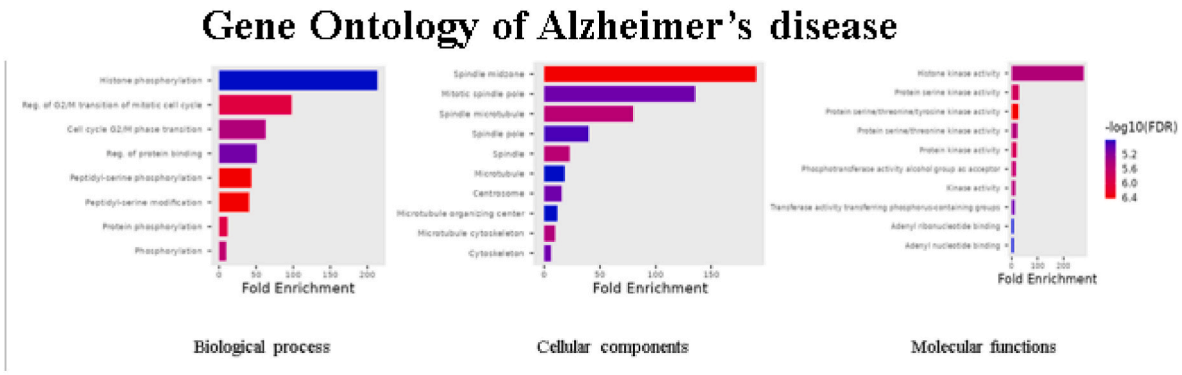

(B)

Fig. 10. (A) The bar chat representation of gene ontology for the shared targets among coronary artery associated targets and the predicted targets of *Tordylium apulum*. (B)The bar chat representation of gene ontology for the shared targets among Alzheimer's disease associated targets and the predicted targets of *Tordylium apulum*.

Similarly, the most important common interacting residues between the cocrystal ligand in the CDK2 crystal complex (Fig. 3C) (PDB ID: 6GUE) (Wood et al., 2019) and kaempferol 3-rutinoside-7-rhamnoside in the docking complex of CDK2 were Asp86 (H-bond in both complexes), Gln131 (H-bond in the docking complex, and van der Waals interaction in the crystal structure), ILE10 (backbone H-bond in the docking complex and hydrophobic interaction in the crystal complex (Fig. 5D). Finally, Cys108 formed 2 H-bonds deep inside the binding site of TRAF2 in both the crystal complex (Fig. 3E) and the docking complex (Fig. 5F). Other important common interacting residues include Glu69 (H-bond in the docking complex but van der Waals interaction in the crystal complex); Val31, Leu73, MET105, Phe108, Val170, Phe172 and more, all engaged in hydrophobic interaction, as well as van der Waals interactions with Lys54, Glu106, Asp115, and Asp171 (Fig. 5E and F).

3.9. Network pharmacology

Using SwissTargetPredictions, we conducted analysis aimed at identifying potential targets with 63 unique compounds maintaining a probability score threshold of at least 0.10. It was intentional that this criterion for selection cover a broad spectrum of potential targets that are pertinent to the compounds being studied. Based on our research, those 63 compounds were linked to 811 distinct targets. Furthermore, we discovered 4610 and 4401 targets using data from the Open Target Platform that were specifically focused on Alzheimer's and Coronary Artery Disease. Of these, 166 and 55 targets were filtered based on an overall association score of equal to or greater than 0.50. Through Venn diagram analysis, we have identified 29 common targets shared between *T. apulum* and the diseases (Fig. 6). The Compound-Target Network was established for *T. apulum* and its associated disorders, both individually and collectively (Fig. 7). The compound-target network of *T. apulum* and Coronary artery exhibited a well-connected topology with 587 nodes and 1034 edges. The Alzheimer's disease network consisted of 492 nodes and 923 edges. Lastly, the network involving *T. apulum* and both diseases included 622 nodes and 1089 edges. Each network (Compound-target coronary artery disease, Compound-target Alzheimer and Compound-target both) displayed substantial interconnectedness, with average values of 3.523, 3.752, and 3.502, respectively. The network density for all three networks is 0.003, 000.4, and 0.003. This metric quantifies the ratio of actual edges to expected edges. Among all three Compound-Target networks, 9,10,18-TriHOME and 4-Hydroxycoumarin exhibit the highest degree of connection, with scores of 106 and 102, respectively. Similarly, when considering target proteins, CA2 and CA12 exhibited the greatest level of connection, with degree of 22 and 21, respectively. The physicochemical and pharmacokinetic properties of the *T. apulum* compounds were analyzsed using Swiss ADME tool. According to Veber's rule total polar surface should be less than or equal to 140 Å and number of rotatable bonds should less than or equal to 10 Kaempferol -deoxyhexose -pentose and Apigenin-di-hexoside have 39 rotatable bonds with 144.19 Å TPSA which indicates that they have poor bioavailability whereas p-Coumaroyl quinic acid has 5 rotatable bonds and 5-O-Feruloylquinic acid has 6 rotatable, both sharing TPSA of 40.46 Å which is optimized bioavailability. *p*-Coumaroyl quinic acid has 6.29 synthetic accessibility and above-mentioned remaining compounds holds the score of 6.3 and this indicates, all of them are reasonably hard to make artificially. Except of *p*-Coumaroyl quinic acid, remaining three

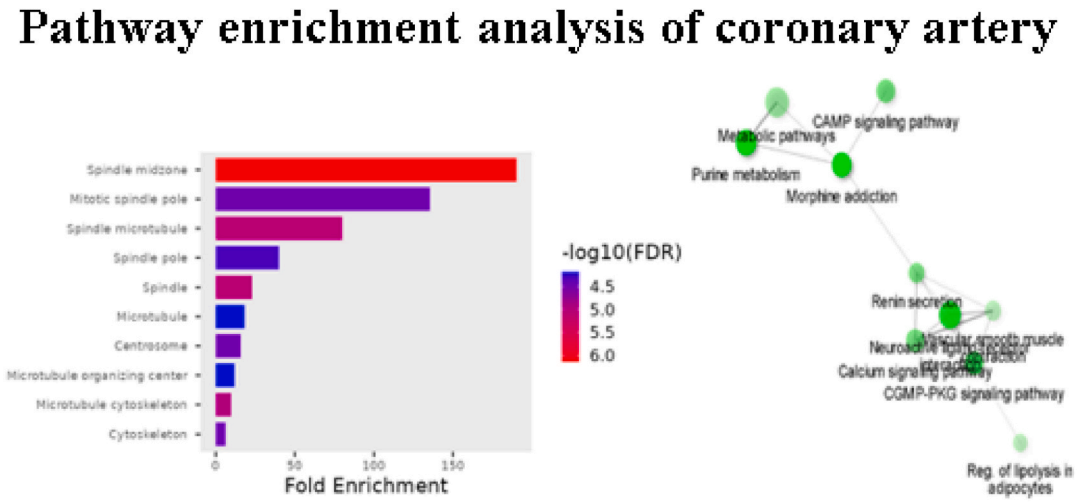

(A)

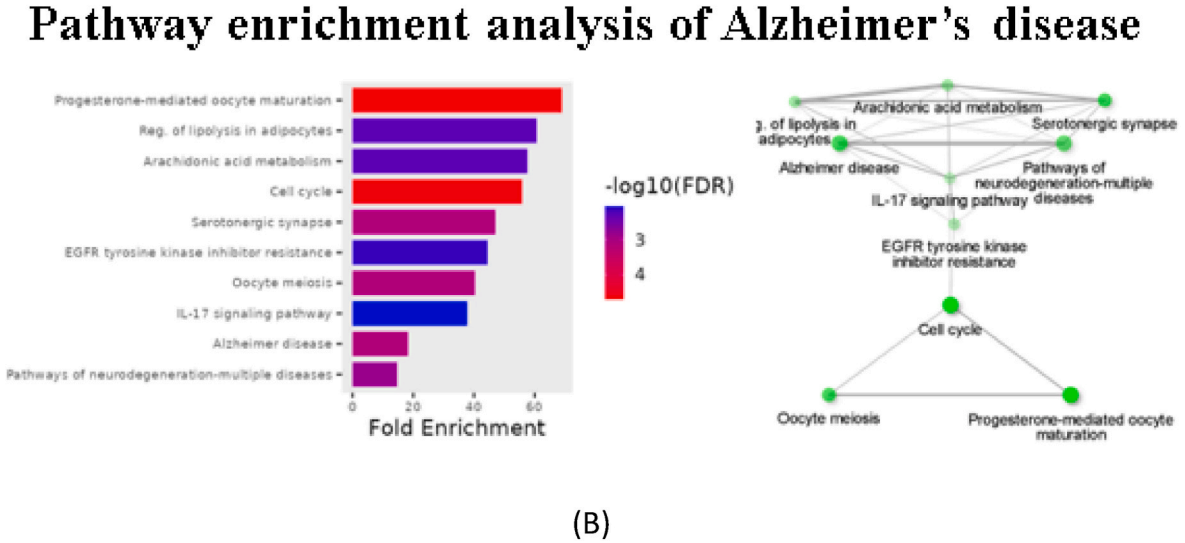

(B)

Fig. 11. (A) Visualization of pathway enrichment analysis for the common set of the shared targets among the coronary artery disease-associated targets and the predicted targets of *Tordylium apulum* compounds, A bar chart of KEGG pathway, pathway network where node size represents no of genes associated with the pathway and thickness of edges represents the percentage of overlapping genes. (B) Visualization of pathway enrichment analysis for the common set of the shared targets among the Alzheimer's disease-associated targets and the predicted targets of *Tordylium apulum* compounds. A bar chart of KEGG pathway, pathway network where node size represents no of genes associated with the pathway and thickness of edges represents the percentage of overlapping genes.

of them possess high GI absorption, notably no absorption in other pharmacokinetics aspects.

Subsequently, the protein-protein interaction network was constructed for two sets of targets: 29 targets for coronary artery and 13 targets for Alzheimer (Fig. 8). The confidence criterion for apparent connection was set at medium confidence >0.4 for coronary artery disease and Alzheimer, as depicted. Both networks were imported into Cytoscape for the analysis of the protein-protein interaction (PPI) analysis. PPI network of coronary artery disease consists of 27 nodes and 44 edges, with an average of 3.259 neighbors per node, on the other hand, PPI network for Alzheimer has 12 nodes and 29 edges, with an average of 4.833 neighbors per node. Furthermore, the network density for each of them was 0.125 and 0.439, while their characteristic path lengths were 3.758 and 1.803, respectively. The nodes in the networks exhibited clustering, with clustering coefficients of 0.420 and 0.651, indicating the existence of coherent protein communities. The Cytohubba plug-in was used to identify hub genes. The parameters were set to display the top 10 hub genes. The results showed the top 10 targets for Coronary artery were F2, SLC29A1, ADDRA2A, PDE5A, ITGA2B, AGTR1, PDE1B, PPARA, ITGB3, and PTGS2 (Fig. 9). The top 10 target for Alzheimer's disease were PTGS1, PTGS2, CDK5, GSK3B, APP, CDC25B, PLK1, AURKA, and AURKE (Fig. 9).

We have performed an extensive analysis on gene ontology to obtain in-depth knowledge on different features including biological processes, cellular components, molecular activities, and their associated pathways using KEGG (Kanehisa et al., 2023). Bar charts are used to visually represent the gene ontology of the disease. Fig. 10 displays the bar charts for the disease, with 166 targets and 55 targets respectively. The bar chart illustrates the degree of enrichment in various paths, with the top 10 pathways being displayed. The size and color correspond to the

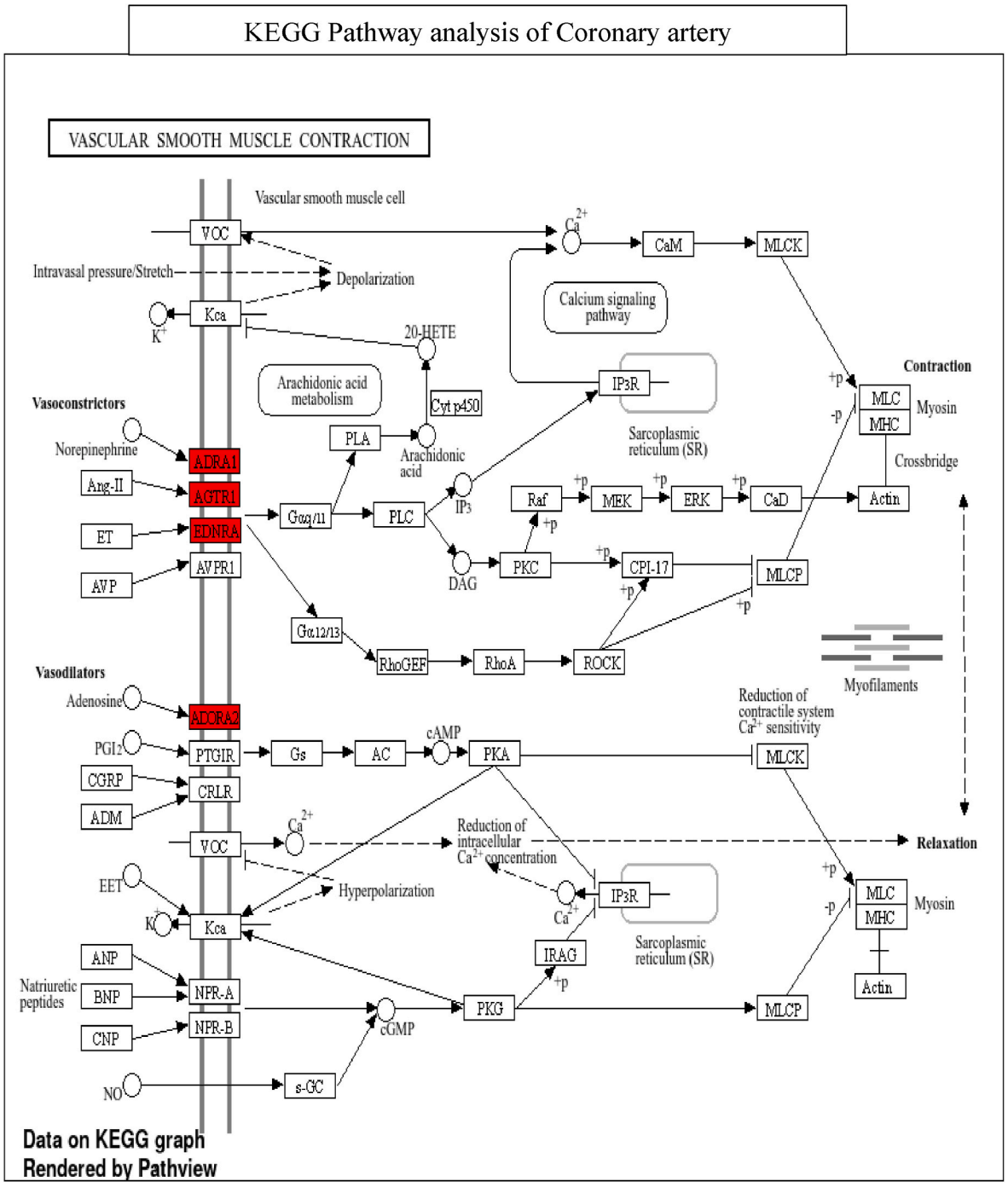

Fig. 12. KEGG pathway of Vascular smooth muscles contraction, the highlighted targets were the site of action of *Tordylium apulum* compound.

number of genes and the negative logarithm of the False Discovery Rate (-log10FDR) respectively. In terms of the biological process, the Cyclic nucleotide catabolic process has the lowest -log10FDR value in the coronary artery disease target sets, whereas Histone phosphorylation has the lowest -log10FDR value in the Alzheimer target sets. Similarly, in cellular components, the coronary artery disease set of targets includes integral components of the synaptic membrane, as well as the leading-edge membrane. The Alzheimer set of targets includes the spindle midzone. Similarly, in molecular function pathways, there is the presence of G protein-coupled adenosine receptor activity and histone kinase activity in their respective target sets (Fig. 11).

The enrichment analysis results indicate that compounds from *T. apulum* are involved in various pathways, including Neuroactive Ligand Receptor Interaction and Vascular Smooth Muscle Contraction pathways. GSK3B is a constituent of the Alzheimer's disease pathway and has a role in phosphorylating the tau protein (Chidambaram & Chinnathambi, 2020) (Fig. 12). The Amyloid precursor protein (APP) is crucial in the development of Alzheimer's disease. The APP gene is situated on chromosome 21 in humans and produces three main isoforms by alternative splicing (Goate et al., 1991). The APP isoform is raised in the brain of individuals with Alzheimer's disease (AD) and is linked to an increase in the deposition of Beta amyloid. This deposition is considered a contributing component in the development of Alzheimer's disease (Menendez-Gonzalez et al., 2006). Vascular smooth muscles are located in the arterial walls, including the coronary arteries. Adenosine, a powerful coronary vasodilator, is synthesized in cardiac myocytes by the

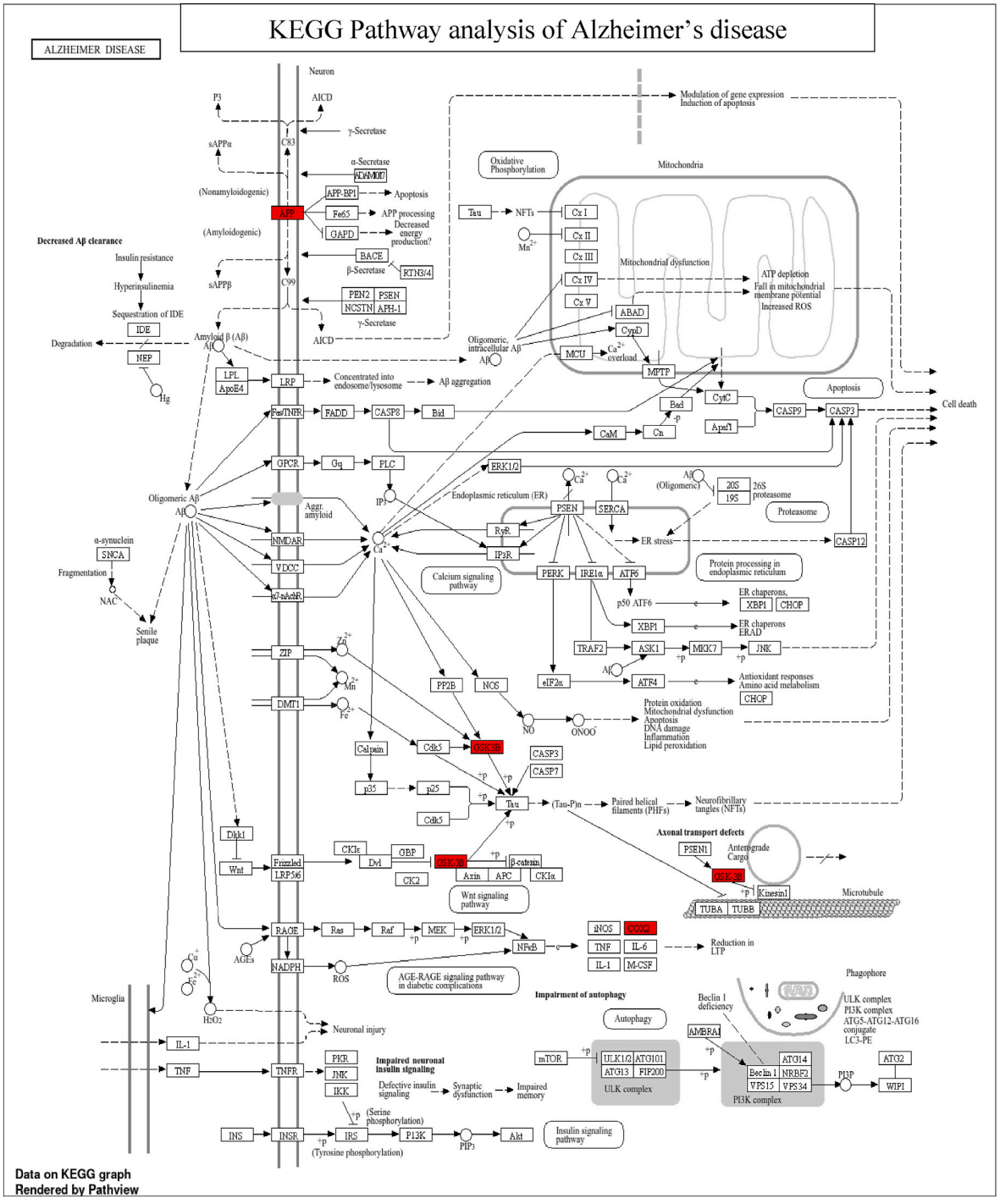

Fig. 13. KEGG pathway of Alzheimer's disease, the highlighted targets were the site of action of *Tordylium apulum* compound.

breakdown of adenine nucleotides (Traverse et al., 2007).

ADORA2A and ADORA1 are involved in the pathway that regulates the contraction of vascular smooth muscle. ADORA2A indirectly affects cardiac contractility by influencing the antiadrenergic effect of ADORA1, as depicted in Fig. 13. ADORA2A and GSK3B are two of the many genes referred to as "hug genes". The common targets and their interactions with the coronary artery and Alzheimer's disease are as follows.

- *p*-Coumaroyl-D-glucose, p-Coumaroyl quinic acid, O-Feruloylquinic acid and Catechin-4-ol 3-*O*-*β*-D-hexopyranoside interacts with APP
- Hydroxycoumarin and Pentahydroxyisoflavone interacts with GSK3B
- N-(1-Deoxy-1-fructosyl)proline, Hydroxycoumarin, Plumieride. Catechin-4-ol 3-*O*-*β*-D-hexopyranoside and Pentahydroxyisoflavone interacts with ADORA2A.
- *p*-Coumaroyl quinic acid and *O*-Feruloylquinic acid are interacting with PDE1B, PDE4D, PDE9A and PDE5A.
- Apigenin-di-hexoside interacts with XDH and ADORA1

Our analysis demonstrates that through *in-silico* evidence of *T. apulum* compounds modulating ligand receptor interactions. Additionally, our study emphasizes the crucial function of APP as a co-factor

in Alzheimer's disease and ADORA2A in coronary artery disease, offering a potential opportunity for intervention. Moreover, the role of GSK3B in Alzheimer's disease is reaffirmed, underscoring its importance in the disease pathway. These findings collectively illustrate the efficacy of network analysis in identifying crucial biological participants and prospective therapeutic targets for complex diseases, thus facilitating more efficient and focused drug development.

4. Conclusions

In conclusion, the study highlights the diverse biological of the aerial parts of *T. apulum* extract, sourced from Turkish flora. Various solvent extracts demonstrated significant differences in their phenolic, flavonoid, and antioxidant contents, with ethanol and water extracts notably exhibiting superior antioxidant activities. The extracts also displayed promising inhibitory effects against AChE, BChE, tyrosinase, and hCA I and hCA II. In addition, the extracts showed significant antimicrobial activity, particularly against the biofilm of pathogens. All tested extracts showed strong anti-cancer properties, in particular the water extract induced apoptosis in HELA cell lines. Molecular docking and network pharmacology revealed the interaction between chemical components and biological effects. Based on these findings, *T. apulum* can be considered as a versatile agent for developing functional applications including pharmaceuticals and nutraceuticals. The results may open new avenues for further research aimed at elucidating the active components in *T. apulum* extracts and their effects in *in vivo* systems.

CRediT authorship contribution statement

Nilofar: Writing – review & editing, Writing – original draft, Methodology, Investigation, Data curation, Conceptualization, Writing – review & editing, Writing – original draft, Methodology, Investigation, Data curation, Conceptualization. **Gokhan Zengin:** Writing – review & editing, Supervision, Methodology, Investigation, Data curation, Conceptualization. **Abdullahi Ibrahim Uba:** Writing – original draft, Visualization, Methodology, Investigation, Data curation. **Nurgul Abul:** Writing – original draft, Methodology, Investigation, Data curation. **Ilhami Gulcin:** Writing – original draft, Methodology, Investigation, Conceptualization. **Ismail Koyuncu:** Writing – original draft, Methodology, Investigation. **Ozgur Yuksekdag:** Writing – original draft, Methodology, Investigation. **Sathish Kumar M Ponnaiya:** Writing – original draft, Visualization, Validation, Methodology, Investigation. **Surendar Tessappan:** Writing – original draft, Visualization, Validation, Methodology, Investigation. **Filomena Nazzaro:** Writing – review & editing, Writing – original draft, Methodology, Investigation. **Florinda Fratianni:** Writing – original draft, Visualization, Methodology, Investigation. **Francesca Coppola:** Writing – original draft, Validation, Methodology, Investigation. **Alina Kalyniukova:** Writing – original draft, Methodology, Investigation, Data curation. **Gizem Emre:** Resources, Methodology, Investigation. **Vasil Andruch:** Writing – original draft, Validation, Methodology, Investigation.

Declaration of competing interest

The authors declare that there are no conflicts of interest.

Data availability

Data will be made available on request.

Appendix A. Supplementary data

Supplementary data to this article can be found online at https://doi.org/10.1016/j.fbio.2024.105088.

References

Aakko, J., Pietilä, S., Toivonen, R., Rokka, A., Mokkala, K., Laitinen, K., Elo, L., & Hänninen, A. (2020). A carbohydrate-active enzyme (CAZy) profile links successful metabolic specialization of prevotella to its abundance in gut microbiota. *Scientific Reports, 10*, Article 12411.

Ahmed, S., Sinan, K. I., Nilofar, C., Ferrante, C., Eyupoğlu, O. E., Etienne, O. K., & Zengin, G. (2023). Online-HPLC strategies, antioxidant and enzyme inhibitory activities of different extracts of *Mondia whitei* leaves. *Journal of Biological Regulators & Homeostatic Agents, 37*, 6029–6039.

Akıncıoğlu, A., Topal, M., Gülçin, İ., & Göksu, S. (2014). Novel sulphamides and sulphonamides incorporating the tetralin scaffold as carbonic anhydrase and acetylcholine esterase inhibitors. *Archiv der Pharmazie, 347*, 68–76.

Altemimi, A., Lakhssassi, N., Baharlouei, A., Watson, D. G., & Lightfoot, D. A. (2017). Phytochemicals: Extraction, isolation, and identification of bioactive compounds from plant extracts. *Plants, 6*, 42.

Anwar, F., & Przybylski, R. (2012). Effect of solvents extraction on total phenolics and antioxidant activity of extracts from flaxseed (*Linum usitatissimum* L.). *Acta Scientiarum Polonorum Technologia Alimentaria, 11*, 293–302.

Ayna, A., Tunc, A., Özbolat, S. N., Bengü, A.Ş., Aykutoğlu, G., Canli, D., Polat, R., Ciftci, M., & Darendelioğlu, E. (2021). Anticancer, and antioxidant activities of royal jelly on HT-29 colon cancer cells and melissopalynological analysis. *Turkish Journal of Botany, 45*, 809–819.

Azwanida, N. (2015). A review on the extraction methods use in medicinal plants, principle, strength and limitation. *Medicinal & Aromatic Plants, 4*, 2167, 0412.

Banjarnahor, S. D., & Artanti, N. (2014). Antioxidant properties of flavonoids. *Medical Journal of Indonesia, 23*, 239–244.

Barthomeuf, C., Grassi, J., Demeule, M., Fournier, C., Boivin, D., & Béliveau, R. (2005). Inhibition of P-glycoprotein transport function and reversion of MDR1 multidrug resistance by cnidiadin. *Cancer Chemotherapy and Pharmacology, 56*, 173–181.

Bernhoft, A. (2010). A brief review on bioactive compounds in plants. *Bioactive compounds in plants-benefits and risks for man and animals, 50*, 11–17.

Bjørklund, G., & Chirumbolo, S. (2017). Role of oxidative stress and antioxidants in daily nutrition and human health. *Nutrition, 33*, 311–321.

Chidambaram, H., & Chinnathambi, S. (2020). G-protein coupled receptors and tau-different roles in Alzheimer's disease. *Neuroscience, 438*, 198–214.

Christou, A., Stavrou, C., Michael, C., Botsaris, G., & Goulas, V. (2024). New insights into the potential inhibitory effects of native plants from Cyprus on pathogenic bacteria and diabetes-related enzymes. *Microbiology Research, 15*, 926–942.

Cincin, Z. B., Unlu, M., Kiran, B., Bireller, E. S., Baran, Y., & Cakmakoglu, B. (2014). Molecular mechanisms of quercitrin-induced apoptosis in non-small cell lung cancer. *Archives of Medical Research, 45*, 445–454.

Daina, A., Michielin, O., & Zoete, V. (2019). SwissTargetPrediction: Updated data and new features for efficient prediction of protein targets of small molecules. *Nucleic Acids Research, 47*, W357–W364.

Dileep, K. V., Ihara, K., Mishima-Tsumagari, C., Kukimoto-Niino, M., Yonemochi, M., Hanada, K., Shirouzu, M., & Zhang, K. Y. J. (2022). Crystal structure of human acetylcholinesterase in complex with tacrine: Implications for drug discovery. *International Journal of Biological Macromolecules, 210*, 172–181.

Dogan, Y., Baslar, S., Ay, G., & Mert, H. H. (2004). The use of wild edible plants in western and central Anatolia (Turkey). *Economic Botany, 58*, 684–690.

Duran, T., Tuncer, Z., Kalyniukova, A., Hradecký, J., Bouyahya, A., Uba, A. I., Senkardes, I., Ponniya, S. K. M., & Zengin, G. (2024). Constituents of alexander's celery (*Smyrnium olusatrum*) extracts and their antioxidant, enzyme inhibitory and anticancer effects based on *in vitro, in silico* and network pharmacology methods. *Journal of Molecular Liquids, 409*, Article 125414.

Elks, J., & Ganellin, C. R. (1990). *Dictionary of drugs*.

Fouzder, C., Mukhuty, A., & Kundu, R. (2021). Kaempferol inhibits Nrf2 signalling pathway via downregulation of Nrf2 mRNA and induces apoptosis in NSCLC cells. *Archives of Biochemistry and Biophysics, 697*, Article 108700.

Fratianni, F., Amato, G., d'Acierno, A., Ombra, M. N., De Feo, V., Coppola, R., & Nazzaro, F. (2023). *In vitro* prospective healthy and nutritional benefits of different *Citrus monofloral* honeys. *Scientific Reports, 13*, 1088.

Gardelly, M., Trimech, B., Horchani, M., Znati, M., Jannet, H. B., & Romdhane, A. (2021). Anti-tyrosinase and anti-butyrylcholinesterase quinolines-based coumarin derivatives: Synthesis and insights from molecular docking studies. *Chemistry Africa, 4*, 491–501.

Ge, S. X., Jung, D., & Yao, R. (2020). ShinyGO: A graphical gene-set enrichment tool for animals and plants. *Bioinformatics, 36*, 2628–2629.

Ghirardini, M. P., Carli, M., Del Vecchio, N., Rovati, A., Cova, O., Valigi, F., Agnetti, G., Macconi, M., Adamo, D., & Traina, M. (2007). The importance of a taste. A comparative study on wild food plant consumption in twenty-one local communities in Italy. *Journal of Ethnobiology and Ethnomedicine, 3*, 1–14.

Giacobini, E. (2003). Cholinesterases: New roles in brain function and in Alzheimer's disease. *Neurochemical Research, 28*, 515–522.

Goate, A., Chartier-Harlin, M.-C., Mullan, M., Brown, J., Crawford, F., Fidani, L., Giuffra, L., Haynes, A., Irving, N., & James, L. (1991). Segregation of a missense mutation in the amyloid precursor protein gene with familial Alzheimer's disease. *Nature, 349*, 704–706.

Gonçalves-Pereira, M., Verdelho, A., Prina, M., Marques, M. J., & Xavier, M. (2021). How many people live with dementia in Portugal? A discussion paper of national estimates. *Portuguese Journal of Public Health, 39*, 58–68.

Grochowski, D. M., Uysal, S., Aktumsek, A., Granica, S., Zengin, G., Ceylan, R., Locatelli, M., & Tomczyk, M. (2017). In vitro enzyme inhibitory properties, antioxidant activities, and phytochemical profile of *Potentilla thuringiaca*. *Phytochemistry Letters, 20*, 365–372.

Guarrera, P., & Savo, V. (2016). Wild food plants used in traditional vegetable mixtures in Italy. *Journal of Ethnopharmacology, 185*, 202–234.
Gülçin, İ., Beydemir, Ş., & Büyükokuroğlu, M. E. (2004). *In vitro* and *in vivo* effects of dantrolene on carbonic anhydrase enzyme activities. *Biological and Pharmaceutical Bulletin, 27*, 613–616.
Hadjichambis, A. C., Paraskeva-Hadjichambi, D., Della, A., Elena Giusti, M., De Pasquale, C., Lenzarini, C., Censorii, E., Reyes Gonzales-Tejero, M., Patricia Sanchez-Rojas, C., & Ramiro-Gutierrez, J. M. (2008). Wild and semi-domesticated food plant consumption in seven circum-Mediterranean areas. *International Journal of Food Sciences & Nutrition, 59*, 383–414.
Hampel, H., Mesulam, M.-M., Cuello, A. C., Farlow, M. R., Giacobini, E., Grossberg, G. T., Khachaturian, A. S., Vergallo, A., Cavedo, E., & Snyder, P. J. (2018). The cholinergic system in the pathophysiology and treatment of Alzheimer's disease. *Brain, 141*, 1917–1933.
Hassan, M. I., Shajee, B., Waheed, A., Ahmad, F., & Sly, W. S. (2013). Structure, function and applications of carbonic anhydrase isozymes. *Bioorganic & Medicinal Chemistry, 21*, 1570–1582.
Jideani, A. I., Silungwe, H., Takalani, T., Omolola, A. O., Udeh, H. O., & Anyasi, T. A. (2021). Antioxidant-rich natural fruit and vegetable products and human health. *International Journal of Food Properties, 24*, 41–67.
Kanehisa, M., Furumichi, M., Sato, Y., Kawashima, M., & Ishiguro-Watanabe, M. (2023). KEGG for taxonomy-based analysis of pathways and genomes. *Nucleic Acids Research, 51*, D587–D592.
Kaplan, A. (2021). GC-MS profiling, antioxidant, antimicrobial activities, DNA cleavage effect of *Symphytum aintabicum* Hub.-Mor. & Wickens (Boraginaceae) and its anticancer activityon MCF-7 cell line. *Turkish Journal of Botany, 45*, 750–764.
Kim, S., Chen, J., Cheng, T., Gindulyte, A., He, J., He, S., Li, Q., Shoemaker, B. A., Thiessen, P. A., & Yu, B. (2023). PubChem 2023 update. *Nucleic Acids Research, 51*, 1373–1380.
Knez, D., Diez-Iriepa, D., Chioua, M., Gottinger, A., Denic, M., Chantegreil, F., Nachon, F., Brazzolotto, X., Skrzypczak-Wiercioch, A., Meden, A., Pišlar, A., Kos, J., Žakelj, S., Stojan, J., Sałat, K., Serrano, J., Fernández, A. P., Sánchez-García, A., Martínez-Murillo, R., … Marco-Contelles, J. (2023). 8-Hydroxyquinolylnitrones as multifunctional ligands for the therapy of neurodegenerative diseases. *Acta Pharmaceutica Sinica B, 13*, 2152–2175.
Koffi, E., Sea, T., Dodehe, Y., & Soro, S. (2010). Effect of solvent type on extraction of polyphenols from twenty three Ivorian plants. *Journal of Animal & Plant Sciences, 5*, 550–558.
Kofinas, C., Chinou, J., Harvala, A., & Gally, A. (1993). Composition and antibacterial activity of the essential oil of *Tordylium apulum* L. *Journal of Essential Oil Research, 5*, 33–36.
Kofinas, C., Chinou, I., Loukis, A., Harvala, C., Maillard, M., & Hostettmann, K. (1998). Flavonoids and bioactive coumarins of *Tordylium apulum*. *Phytochemistry, 48*, 637–641.
Kofinas, C., Chinou, I., Loukis, A., Harvala, C., Roussakis, C., Maillard, M., & Hostettmann, K. (1998). Cytotoxic coumarins from the aerial parts of *Tordylium apulum* and their effects on a non-small-cell bronchial carcinoma line. *Planta Medica, 64*, 174–176.
Kucukoglu, K., Gul, H. I., Taslimi, P., Gulcin, I., & Supuran, C. T. (2019). Investigation of inhibitory properties of some hydrazone compounds on hCA I, hCA II and AChE enzymes. *Bioorganic Chemistry, 86*, 316–321.
Kurumbail, R. G., Stevens, A. M., Gierse, J. K., McDonald, J. J., Stegeman, R. A., Pak, J. Y., Gildehaus, D., iyashiro, J. M., Penning, T. D., Seibert, K., Isakson, P. C., & Stallings, W. C. (1996). Structural basis for selective inhibition of cyclooxygenase-2 by anti-inflammatory agents. *Nature, 384*, 644–648.
Lazarova, I., Nilofar, Caprioli, G., Piatti, D., Ricciutelli, M., Ulusan, M. D., Koyuncu, I., Yuksekdag, O., Mollica, A., & Stefanucci, A. (2024). Influence of extraction solvents on the chemical constituents and biological activities of *Astragalus aduncus* from Turkey flora: *In vitro* and *in silico* insights. *Archiv der Pharmazie*, Article e2400257.
Luczaj, L., Pieroni, A., Tardío, J., Pardo-de-Santayana, M., Sõukand, R., Svanberg, I., & Kalle, R. (2012). Wild food plant use in 21st century europe: The disappearance of old traditions and the search for new cuisines involving wild edibles. *Acta Societatis Botanicorum Poloniae, 81*, 359–370.
Maresca, V., Vaglica, A., Ilardi, V., Bruno, M., & Basile, A. (2024). Chemical composition and antioxidant activities of the essential oil of *Tordylium apulum* L. collected in Sicily. *Natural Product Research, 38*, 2026–2030.
Martínez-Rosell, G., Giorgino, T., & De Fabritiis, G. (2017). Playmolecule protein prepare: A web application for protein preparation for molecular dynamics simulations. *Journal of Chemical Information and Modeling, 57*, 1511–1516.
Matejic, J. S., Dzamic, A. M., Mihajilov-Krstev, T. M., Randelovic, V. N., Krivosej, Z. A., & Marin, P. D. (2013). Total phenolic and flavonoid content, antioxidant and antimicrobial activity of extracts from *Tordylium maximum*. *Journal of Applied Pharmaceutical Science, 3*, 55–59.
Menendez-Gonzalez, M., Pérez-Pinera, P., Martinez-Rivera, M., Calatayud, M., & Blazquez Menes, B. (2006). APP processing and the APP-KPI domain involvement in the amyloid cascade. *Neurodegenerative Diseases, 2*, 277–283.
Morris, G. M., Huey, R., Lindstrom, W., Sanner, M. F., Belew, R. K., Goodsell, D. S., & Olson, A. J. (2009). AutoDock4 and AutoDockTools4: Automated docking with selective receptor flexibility. *Journal of Computational Chemistry, 30*, 2785–2791.
Nahoum, V., Roux, G., Anton, V., Rouge, P., Puigserver, A., Bischoff, H., Henrissat, B., & Payan, F. (2000). Crystal structures of human pancreatic alpha-amylase in complex with carbohydrate and proteinaceous inhibitors. *Biochemical Journal, 346*, 201–208.
Nar, M., Çetinkaya, Y., Gülçin, İ., & Menzek, A. (2013). (3, 4-Dihydroxyphenyl)(2, 3, 4-trihydroxyphenyl) methanone and its derivatives as carbonic anhydrase isoenzymes inhibitors. *Journal of Enzyme Inhibition and Medicinal Chemistry, 28*, 402–406.
Ngo, T. V., Scarlett, C. J., Bowyer, M. C., Ngo, P. D., & Vuong, Q. V. (2017). Impact of different extraction solvents on bioactive compounds and antioxidant capacity from the root of *Salacia chinensis* L. *Journal of Food Quality, 2017*, Article 9305047.
Nilofar, Duran, T., Uba, A. I., Cvetanović Kljakić, A., Božunović, J., Gašić, U., Bouyahya, A., Yıldiztugay, E., Ferrante, C., & Zengin, G. (2024). Extractions of aerial parts of *Hippomarathrum scabrum* with conventional and green methodologies: Chemical profiling, antioxidant, enzyme inhibition, and anti-cancer effects. *Journal of Separation Science, 47*, Article 2300678.
Omer, H. A. A., Caprioli, G., Abouelenein, D., Mustafa, A. M., Uba, A. I., Ak, G., Ozturk, R. B., Zengin, G., & Yagi, S. (2022). Phenolic Profile, antioxidant and enzyme inhibitory activities of leaves from two *Cassia* and two *Senna* Species. *Molecules, 27* (17), 5590.
Organization, W. H. (2007). A global health guardian: Climate change, air pollution and antimicrobial resistance. *WHO, ten years in public health, 2017*, 136–142.
Orhan, I. E., Tosun, F., Deniz, F. S. S., Eren, G., Mıhoğlugil, F., Akalgan, D., & Miski, M. (2021). Butyrylcholinesterase-inhibiting natural coumarin molecules as potential leads. *Phytochemistry Letters, 44*, 48–54.
Orhan, I. E., Tosun, F., & Skalicka-Woźniak, K. (2016). Cholinesterase and tyrosinase inhibitory, and antioxidant potential of randomly selected Umbelliferous plant species and the chromatographic profile of *Heracleum platytaenium* Boiss. and *Angelica sylvestris* L. var. *sylvestris*. *Journal of the Serbian Chemical Society, 81*, 357–368.
Osek, J., & Wieczorek, K. (2022). Listeria monocytogenes-how this pathogen uses its virulence mechanisms to infect the hosts. *Pathogens, 11*.
Özbey, F., Taslimi, P., Gülçin, İ., Maraş, A., Göksu, S., & Supuran, C. T. (2016). Synthesis of diaryl ethers with acetylcholinesterase, butyrylcholinesterase and carbonic anhydrase inhibitory actions. *Journal of Enzyme Inhibition and Medicinal Chemistry, 31*, 79–85.
Özek, T., Kürkcüoglu, M., Baser, K. H. C., & Tosun, A. (2007). Composition of the essential oils of Tordylium trachycarpum (Boiss.) Al-Eisawi et Jury and *Tordylium hasselquistiae* DC. growing in Turkey. *Journal of Essential Oil Research, 19*, 410–412.
Pettersen, E. F., Goddard, T. D., Huang, C. C., Couch, G. S., Greenblatt, D. M., Meng, E. C., & Ferrin, T. E. (2004). UCSF Chimera—a visualization system for exploratory research and analysis. *Journal of Computational Chemistry, 25*, 1605–1612.
Pieroni, A., Janiak, V., Dürr, C., Lüdeke, S., Trachsel, E., & Heinrich, M. (2002). *In vitro* antioxidant activity of non-cultivated vegetables of ethnic Albanians in southern Italy. *Phytotherapy Research*, 467–473.
Ponnanikajamideen, M., Rajeshkumar, S., Vanaja, M., & Annadurai, G. (2019). *In vivo* type 2 diabetes and wound-healing effects of antioxidant gold nanoparticles synthesized using the insulin plant *Chamaecostus cuspidatus* in albino rats. *Canadian Journal of Diabetes, 43*, 82–89. e86.
Rescigno, A., Sollai, F., Pisu, B., Rinaldi, A., & Sanjust, E. (2002). Tyrosinase inhibition: General and applied aspects. *Journal of Enzyme Inhibition and Medicinal Chemistry, 17*, 207–218.
Sasidharan, S., Chen, Y., Saravanan, D., Sundram, K., & Latha, L. Y. (2011). Extraction, isolation and characterization of bioactive compounds from plants' extracts. *African Journal of Traditional, Complementary and Alternative Medicines, 8*, Article 3218439.
Savo, V., Salomone, F., Mattoni, E., Tofani, D., & Caneva, G. (2019). Traditional salads and soups with wild plants as a source of antioxidants: A comparative chemical analysis of five species growing in central Italy. *Evidence-based Complementary and Alternative Medicine, 2019*, Article 6782472.
Shannon, P., Markiel, A., Ozier, O., Baliga, N. S., Wang, J. T., Ramage, D., Amin, N., Schwikowski, B., & Ideker, T. (2003). Cytoscape: A software environment for integrated models of biomolecular interaction networks. *Genome Research, 13*, 2498–2504.
Sinan, K. I., Eyupoglu, O. E., Ferrante, C., Ahmed, S., Etienne, O. K., & Zengin, G. (2024). Multiple online-HPLC methodologies and biological properties of leaves and stem barks extracts of *Chrysanthellum indicum*. *Microchemical Journal, 197*, Article 109847.
Slinkard, K., & Singleton, V. L. (1977). Total phenol analysis: Automation and comparison with manual methods. *American Journal of Enology and Viticulture, 28*, 49–55.
Smith, R. M. (2003). Before the injection—modern methods of sample preparation for separation techniques. *Journal of Chromatography A, 1000*, 3–27.
Souers, A. J., Leverson, J. D., Boghaert, E. R., Ackler, S. L., Catron, N. D., Chen, J., Dayton, B. D., Ding, H., Enschede, S. H., Fairbrother, W. J., Huang, D. C. S., Hymowitz, S. G., Jin, S., Khaw, S. L., Kovar, P. J., Lam, L. T., Lee, J., Maecker, H. L., Marsh, K. C., … Elmore, S. W. (2013). ABT-199, a potent and selective BCL-2 inhibitor, achieves antitumor activity while sparing platelets. *Nature Medicine, 19*, 202–208.
Supuran, C. T., & Scozzafava, A. (2007). Carbonic anhydrases as targets for medicinal chemistry. *Bioorganic & Medicinal Chemistry, 15*, 4336–4350.
Szklarczyk, D., Gable, A.L., Lyon, D., Junge, A., Wyder, S., Huerta-Cepas, J., Simonovic, M., Doncheva, N.T., Morris, J.H., & Bork, P. (20199. STRING v11: Protein–protein association networks with increased coverage, supporting functional discovery in genome-wide experimental datasets. Nucleic Acids Research 47, D607-D613.
Tan, C.-C., Yu, J.-T., Wang, H.-F., Tan, M.-S., Meng, X.-F., Wang, C., Jiang, T., Zhu, X.-C., & Tan, L. (2014). Efficacy and safety of donepezil, galantamine, rivastigmine, and memantine for the treatment of Alzheimer's disease: A systematic review and meta-analysis. *Journal of Alzheimer's Disease, 41*, 615–631.
Tirillini, B., Pintore, G., Chessa, M., & Menghini, L. (2006). Essential oil composition of *Tordylium apulum* L. from Italy. *Journal of Essential Oil Research, 18*, 51–52.
Tosun, A., Kürkçüoglu, M., & Başer, K. H. C. (2006). Essential oils of *Tordylium pestalozzae* boiss., T*ordylium pustulosum* boiss. and *Tordylium lanatum* (boiss.) boiss. (Umbelliferae) growing wild in Turkey. *Journal of Essential Oil Research, 18*, 640–642.

Traverse, J.H., Chen, Y., Hou, M., Li, Y., & Bache, R.J. (20079. Effect of K+ ATP channel and adenosine receptor blockade during rest and exercise in congestive heart failure. Circulation Research 100, 1643-1649.

Tugrak, M., Gul, H. I., Demir, Y., Levent, S., & Gulcin, I. (2021). Synthesis and *in vitro* carbonic anhydrases and acetylcholinesterase inhibitory activities of novel imidazolinone-based benzenesulfonamides. *Archiv der Pharmazie, 354*, Article e2000375.

Whang, W. K., Park, H. S., Ham, I., Oh, M., Namkoong, H., Kim, H. K., Hwang, D. W., Hur, S. Y., Kim, T. E., & Park, Y. G. (2005). Natural compounds, fraxin and chemicals structurally related to fraxin protect cells from oxidative stress. *Experimental & Molecular Medicine, 37*, 436–446.

Wong, P. Y., & Kitts, D. D. (2006). Studies on the dual antioxidant and antibacterial properties of parsley (*Petroselinum crispum*) and cilantro (*Coriandrum sativum*) extracts. *Food Chemistry, 97*, 505–515.

Wood, D. J., Korolchuk, S., Tatum, N. J., Wang, L.-Z., Endicott, J. A., Noble, M. E. M., & Martin, M. P. (2019). Differences in the conformational energy landscape of CDK1 and CDK2 suggest a mechanism for achieving selective CDK inhibition. *Cell Chemical Biology, 26*, 121–130.

Yang, L. J., Han, T., Liu, R. N., Shi, S. M., Luan, S. Y., & Meng, S. N. (2024). Plant-derived natural compounds: A new frontier in inducing immunogenic cell death for cancer treatment. *Biomedicine & Pharmacotherapy, 177*, Article 117099.

Yang, C., Song, J., Hwang, S., Choi, J., Song, G., & Lim, W. (2021). Apigenin enhances apoptosis induction by 5-fluorouracil through regulation of thymidylate synthase in colorectal cancer cells. *Redox Biology, 47*, Article 102144.

Zengin, G., Nilofar, Yildiztugay, E., Bouyahya, A., Cavusoglu, H., Gevrenova, R., & Zheleva-Dimitrova, D. (2023). A comparative study on UHPLC-HRMS profiles and biological activities of *Inula sarana* different extracts and its beta-cyclodextrin complex: Effective insights for novel applications. *Antioxidants, 12*, 1842.

Zhang, J., Wu, Y., Li, Y., Li, S., Liu, J., Yang, X., Xia, G., & Wang, G. (2024). Natural products and derivatives for breast cancer treatment: From drug discovery to molecular mechanism. *Phytomedicine, 129*, Article 155600.